Engineering Geology 318 (2023) 107104

Contents lists available at ScienceDirect

Engineering Geology

journal homepage: www.elsevier.com/locate/enggeo

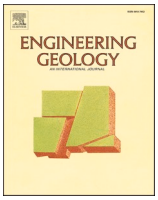

Improving the spatial control of soil biocementation using indigenous microorganisms: Column experiments and reactive transport modeling

Minyong Lee [a], Michael G. Gomez [b,*], Charles M.R. Graddy [c], Alexandra C.M. San Pablo [d], Jason T. DeJong [d], Douglas C. Nelson [c]

[a] Department of Civil and Environmental Engineering, University of Washington, Seattle, WA 98195, United States of America
[b] Department of Civil and Environmental Engineering, University of Washington, 132G More Hall, Seattle, WA 98195, United States of America
[c] Department of Microbiology and Molecular Genetics, University of California, Davis, CA 95616, United States of America
[d] Department of Civil and Environmental Engineering, University of California, Davis, CA 95616, United States of America

ARTICLE INFO

Keywords:
Ground Improvement
Microbially Induced Calcite Precipitation (MICP)
Biocementation
Reactive Transport
Biostimulation
Sands

ABSTRACT

Microbially-Induced Calcite Precipitation (MICP), or biocementation, is a biomediated soil improvement process that uses microbial ureolytic activity to enable the precipitation of $CaCO_3$ on soil particle surfaces and contacts. As the technology advances towards practical adoption, approaches that can modulate the spatial uniformity of biocementation and maximize treatment extent will be critical towards reducing implementation costs and impacts. In this study, treatment strategies capable of enriching indigenous ureolytic microorganisms at controlled ureolytic activities and the effects of these techniques on resulting spatial distributions of MICP were explored using centimeter- and meter-scale soil column experiments and reactive transport simulations. In column experiments, differences in treatment solution supplied yeast extract concentrations were shown to reliably control the enrichment of indigenous ureolytic microorganisms and achieve a wide range of ureolytic activities. Reactive transport simulations further demonstrated that reductions in stimulated ureolytic rates could enable more uniform improvement and increases in the extent of improvement with reduced sensitivity to changes in solution injection velocities. A reaction-to-injection duration ratio (RTIDR) parameter was proposed and captured the collective impacts of changes in injection rates and ureolytic reaction rates on reactive transport conditions thereby unifying outcomes from both simulations and experiments. A nonuniformity area (NA) parameter was also introduced to quantitatively characterize differences in biocementation uniformity independent of length scale and $CaCO_3$ magnitudes. Results from this study collectively demonstrate the utility of changes in stimulated ureolytic activities towards controlling the spatial uniformity and extent of biocementation over meter-scale distances.

1. Introduction

Geotechnical ground improvement is a 6 billion dollar per year industry in the U.S. (DeJong et al., 2010) that has relied almost exclusively on energy-intensive materials and high mechanical energy to improve problematic soils (Karol, 2003). Over the past two decades, researchers have shown the transformative potential of bio-mediated processes to improve soil engineering behaviors while reducing environmental impacts relative to conventional soil improvement methods (Seagren and Aydilek, 2010; DeJong et al., 2013; DeJong et al., 2022; DeJong and Kavazanjian, 2019; Sharma et al., 2021). One such process, Microbially-induced Calcite Precipitation (MICP), uses microbial urea hydrolysis (ureolysis) to induce the precipitation of calcium carbonate ($CaCO_3$) minerals on soil particle surfaces and contacts (Ferris et al., 1997; Stocks-Fischer et al., 1999; DeJong et al., 2006). The biocementation process can improve the strength and stiffness of soils while also reducing soil porosity and hydraulic conductivity (Montoya and DeJong, 2015; Feng and Montoya, 2016; Gomez et al., 2018a). Potential applications include the modification of subsurface groundwater flow (Cuthbert et al., 2013; Tobler et al., 2014; Minto et al., 2016), erosion and scour prevention (Jiang and Soga, 2017; Montoya et al., 2018; Clarà Saracho et al., 2021), repair of damaged concrete, marble, and limestone

* Corresponding author.
E-mail addresses: my0321@uw.edu (M. Lee), mggomez@uw.edu (M.G. Gomez), cmgraddy@ucdavis.edu (C.M.R. Graddy), amsanpablo@ucdavis.edu (A.C.M. San Pablo), jdejong@ucdavis.edu (J.T. DeJong), dcnelson@ucdavis.edu (D.C. Nelson).

https://doi.org/10.1016/j.enggeo.2023.107104
Received 22 September 2022; Received in revised form 6 December 2022; Accepted 27 March 2023
Available online 31 March 2023

materials (Ramakrishnan et al., 2005; Tziviloglou et al., 2016; Minto et al., 2018), immobilization of divalent groundwater contaminants (Fujita et al., 2008; Kumari et al., 2016; Jiang et al., 2019), improved petroleum extraction and recovery (Ferris et al., 1997; Phillips et al., 2018), and mitigation of earthquake-induced soil liquefaction (Montoya et al., 2013; Xiao et al., 2018; Darby et al., 2019; Zamani and Montoya, 2019; Riveros and Sadrekarimi, 2020; Lee et al., 2022). Soil improvement applications for biocementation have been increasingly explored in recent years through field demonstrations (Gomez et al., 2015; Phillips et al., 2016; Saneiyan et al., 2019; Terzis et al., 2020; Ghasemi and Montoya, 2020) with notable advances in the characterization of the engineering response of biocemented materials (Darby et al., 2019; Nafisi et al., 2020; Riveros and Sadrekarimi, 2020; Lee et al., 2022), process reactive transport numerical modeling (Nassar et al., 2018; Minto et al., 2019), and the use of indigenous soil microorganisms (Fujita et al., 2000; Burbank et al., 2011; Gomez et al., 2017; San Pablo et al., 2020). The process holds significant promise for practical applications; however, challenges have persisted with respect to controlling the spatial distribution and uniformity of MICP at meter-scale (Mujah et al., 2017; DeJong et al., 2022). Treatment extent limitations can be overcome by installing treatment wells at shorter well-to-well spacings, however, such constraints will significantly increase economic and environmental impacts and undermine process advantages. Identification of reliable techniques that can improve the spatial control of the biocementation process may yield transformative benefits once applied at field-scale.

Urea hydrolysis during MICP is most commonly mediated by nonnative ureolytic bacteria such as *Sporosarcina pasteurii* (*S. pasteurii*), which can be introduced into soils at high cell densities prior to cementation injections. Recently, researchers have shown that the biocementation process can be mediated by indigenous ureolytic microorganisms existing in natural geomaterials, including alluvial and marine sands, clays, and groundwater samples, thereby eliminating the need for ex-situ cell culturing and injection (Fujita et al., 2000, 2008; Burbank et al., 2011, 2013; Tobler et al., 2011; Gat et al., 2014, 2016; Gomez et al., 2014; Gomez et al., 2017, 2018b; Lee et al., 2019; Graddy et al., 2018, 2021; Cardoso et al., 2020; Islam et al., 2020; San Pablo et al., 2020; Wang et al., 2020; Safdar et al., 2021). These studies have developed stimulation solutions that impose selective environmental conditions, including alkaline solution pH and high ammonium concentrations, to promote enrichment of ureolytic microorganisms over other non-ureolytic microorganisms which may compete for supplied nutrients (Gomez et al., 2018b). In many of these studies, the rapid accumulation of high bulk ureolytic activity was paramount in stimulation solution design and taken to be indicative of more successful ureolytic enrichment. Although high ureolytic activities may be characteristic of enriched soils that can more rapidly generate biocementation, high urea hydrolysis rates can also dramatically reduce biocementation spatial uniformity when treatment injections are transported at relatively slow velocities (Zambare et al., 2019; Montoya et al., 2021). Such conditions can increase urea hydrolysis and related precipitation reactions during injections and promote greater $CaCO_3$ precipitation near injection sources with more limited transport of reactants to further distances (Gomez et al., 2019; San Pablo et al., 2020). Given the importance of microbial urea hydrolysis rates on reactive transport conditions present during MICP, it is clear that treatment strategies that can reliably control achieved urea hydrolysis rates may provide new opportunities to control the spatial distribution of biocementation for different field-scale treatment scenarios.

Few studies have considered the interplay between ureolytic reaction rates and solution transport rates and their combined impacts on biocementation spatial uniformity (Martinez et al., 2014; Nassar et al., 2018; Zambare et al., 2019; Minto et al., 2019; Montoya et al., 2021) with almost all past studies relying on the mediation of the MICP process using augmented *S. pasteurii* cells. Recent meter-scale experiments suggest that achieving uniform distributions of augmented cell densities may be exceedingly difficult over large injection distances, even in controlled laboratory experiments, due to cell attachment and filtration by porous media, which act to concentrate augmented cells near injection sources (Ginn et al., 2002; Gomez et al., 2017, 2019; San Pablo et al., 2020). However, novel treatment techniques including initial solution pH adjustment (Cheng et al., 2019) and temperature control (Xiao et al., 2021) may afford improvements in the spatial uniformity of augmented MICP through other means. In contrast, the stimulation of indigenous ureolytic microorganisms may eliminate cell transport limitation altogether by enriching microorganisms already distributed throughout soil pore space (Graddy et al., 2018) with the potential for significant economic and environmental benefits relative to augmentation (Gomez et al., 2017). Despite these practical advantages, the ability to regulate achieved stimulated urea hydrolysis rates through treatment solution design has remained poorly understood (San Pablo et al., 2020). Control of bulk ureolytic activity may be difficult in stimulated soils as such materials contain diverse microbial communities where even small changes in solution composition can shift microbial populations dramatically (Graddy et al., 2018, 2021). San Pablo et al. (2020) first demonstrated that changes in applied yeast extract (YE) concentrations could be used to alter reactive transport conditions thereby controlling the spatial distribution of biocementation realized in two 3.67-m-long column experiments treated using identical flow rates. In these experiments, lower supplied YE concentrations reduced stimulated urea hydrolysis rates and enabled improved cementation uniformity. While promising, the ability of ureolytic rates to be reliably and systematically controlled through variations in supplied nutrient concentrations, the potential consequences of such changes on achieved engineering improvements, and the collective impacts of simultaneous changes in ureolytic reaction rates and injection rates on improvement distributions expected at meter-scale remained unexplored.

In this study, twelve centimeter-scale soil column experiments were employed to systematically investigate the ability of novel treatment strategies to enrich natural soils to achieve a wide spectrum of ureolytic rates capable of improving the spatial control of ureolytic biocementation under different field-scale transport conditions. In all experiments, applied stimulation and cementation solutions were modified to contain varying YE concentrations between 0 and 0.2 g/L and resulting effects on stimulated ureolytic rates, soil shear wave velocities (V_s), and soil $CaCO_3$ contents were investigated. Leveraging these experimental insights, a one-dimensional reactive transport model was used to further explore the implications of the achieved ureolytic rates on the distribution of biocementation expected in 3.67-m-long soil column models similar to those physically tested by San Pablo et al. (2020) but subjected to different injection conditions. Relationships between stimulated ureolytic rates, injection rates, and biocementation spatial uniformity and extent were investigated and compared to previous observations by San Pablo et al. (2020) to provide a more comprehensive understanding of the ability of the investigated enrichment techniques to address practical field treatment challenges. Lastly, two new parameters, the reaction-to-injection duration ratio (RTIDR) and the non-uniformity area (NA), were proposed and provide new metrics by which reactive transport conditions and treatment uniformity can be quantified and compared between studies.

2. Materials and methods

2.1. Soil materials

All soil column experiments contained a poorly-graded Concrete Sand material characterized extensively in past biocementation experiments (Gomez et al., 2014; Gomez et al., 2017, 2018b; Lee et al., 2019). The soil was obtained from an alluvial deposit in Woodland, CA, USA and had a D_{10} of 0.23 mm, D_{30} of 0.54 mm, D_{60} of 1.54 mm, fines content of 1.1% by mass, and an e_{min} and e_{max} of 0.35 and 0.60, respectively. The USCS classification for this soil was SP following ASTM D2487–10

(ASTM, 2017). Previous microbiological characterizations of Concrete Sand (Graddy et al., 2018, 2021) have indicated that significant microbial diversity exists in this parent soil, with nearly 20 different strains of *Sporosarcina* identified following sequential enrichment injections.

2.2. Centimeter-scale soil column specimens

Centimeter-scale soil column specimens were prepared in 15.2 cm high, 7.6 cm inner diameter acrylic cylinders that included fittings for bender element V_s sensors and aqueous sampling ports at mid-height (Supplemental Fig. S1). Soil materials were placed in columns in six lifts using moist tamping to obtain a relative density around 55%. All columns had initial porosities of 35% ± 1% and pore volumes (PV) of ≈250 mL. Spring-loaded reaction frames applied a total vertical stress of 100 kPa to all columns that was maintained throughout the treatment process. Following preparation, all columns were saturated with deionized water and remained untreated for 24 h. Four soil columns were tested in experiment set A and eight soil columns were tested in experiment set B.

2.3. Treatment injections

Centimeter-scale soil columns received treatments in three phases: (i) stimulation, (ii) carbonate flushing, and (iii) cementation. For all treatments, injection volumes of 375 mL (≈1.5 PV) were applied at a flow rate of 2.4 PV/h (10 mL/min for a total injection time of 37.5 min). All columns received stimulation solutions once daily for the first 6 days. Stimulation solution compositions followed previous techniques shown to effectively select for ureolytic microorganisms (Gomez et al., 2018b) but included large reductions in supplied urea (350 mM to 50 mM) shown to have no significant effects on stimulation efficacy (San Pablo et al., 2020). All stimulation solutions were pH-adjusted to 9.0 prior to injection and contained 50 mM urea, 42.5 mM sodium acetate, 100 mM ammonium chloride, and varying YE concentrations intended to alter obtained stimulated ureolytic activities. In experiment set A, three columns received daily stimulation treatments with either 0.01, 0.07, or 0.2 g/L YE. A fourth column received alternating daily injections with either 0.07 g/L YE (odd treatments) or 0 g/L YE (even treatments) to explore the effect of alternating nutritionally complete and incomplete treatments on ureolytic activity. In experiment set B, four columns received daily injections with either 0.02, 0.04, 0.08, or 0.2 g/L YE and four columns received alternating daily injections with identical YE concentrations and no YE applied on alternating days. Following six stimulation treatments and immediately before the first cementation injection, all columns received a carbonate "flush" solution that was identical to the stimulation solution but was not pH-adjusted, which was intended to remove high aqueous carbonate concentrations existing within soil columns following stimulation (Gomez et al., 2019).

Subsequently, all columns in experiment set A received 10 cementation treatments and all columns in experiment set B received 9 cementation treatments intended to obtain post-treatment soil $CaCO_3$ contents near 5% by mass (Gomez and DeJong, 2017). Cementation solutions were similar in composition to stimulation solutions but contained calcium chloride and higher urea concentrations as well as reduced initial pH and ammonium concentrations. In experiment set A, cementation solutions were applied once daily and contained 350 mM urea and 250 mM calcium chloride. In experiment set B, cementation solutions were applied once every 48 h to allow for reaction completion to occur in all columns including those with slower ureolytic rates. Experiment set B solutions also contained 250 mM urea and calcium chloride, based on recent experiments that showed urea concentrations could be reduced to be equimolar with calcium chloride without affecting precipitation efficiency (San Pablo et al., 2022). In both experiment sets, the YE additions during cementation treatments were identical to those applied during stimulation treatments and continued to alternate in columns receiving nutritive and non-nutritive treatments. Following cementation, rinse solutions (500 mM calcium chloride, pH-adjusted to 9.0) were applied to all columns to remove soluble by-products (Lee et al., 2019). A summary of all stimulation and cementation solutions for both experiment sets is provided in Supplemental Table S1.

2.4. Aqueous sampling

Solution samples (≈2 mL) were collected from column mid-height sampling ports using sterile syringes and needles before and after each treatment injection and for select injections at various times during solution retention periods to monitor ureolytic rates. In experiment set A, all columns were sampled 2, 4, 8, and 24 h after applying the 2nd, 4th, and 6th stimulation treatment and the 3rd, 6th, 8th, and 10th cementation treatment. In experiment set B, all columns were sampled 2, 4, 8, 24, and 48 h after applying the 2nd and 6th stimulation treatment and the 1st, 5th, and 9th cementation treatment. All samples were stored at −20 °C immediately following collection and remained frozen until analysis.

2.5. Aqueous measurements

Solution pH measurements were completed using a semi-micro pH electrode and meter system (Fisher Scientific, Waltham, MA) that was calibrated daily using a three-point buffer sequence (4.01, 7.00, 10.01) and had ±0.01 pH unit accuracy. Solution urea measurements were completed using a colorimetric urea assay similar to Knorst et al. (1997) wherein a colorimetric reagent consisting of 4% (*w/v*) *p*-Dimethylaminobenzaldehyde and 4% (*v/v*) HCl in 96% ethanol was added to dilute sample volumes. Absorbance values were measured at 422 nm using a microplate spectrophotometer.

2.6. Shear wave velocity measurements

Shear wave velocity measurements were obtained for experiment set B soil columns using piezo-ceramic bender element sensor pairs oriented perpendicular to columns at mid-height. Bender elements were assembled following procedures similar to Montoya et al. (2012) and were isolated from the highly conductive aqueous environment using a multi-step Hysol E-90FL epoxy (Henkel Corp., Düsseldorf, Germany) and electronics wax coating process (Gomez et al., 2017). All transmitting bender elements were excited using a 24-V 100 Hz square wave generated by a signal generator system (National Instruments, Austin, TX) and all received signals were measured and recorded with an oscilloscope (Pico Technology, Tyler, TX) at a sampling frequency of 1 MHz. V_s measurements were completed once daily before injections and velocities were determined from visual interpretation of S-wave arrivals and sensor spacings.

2.7. Soil sampling and $CaCO_3$ content measurements

Following all rinse injections, soil columns were drained, extruded using a hydraulic jack, and oven-dried at 110 °C for at least 48 h. Soil columns were subsampled into four discrete sections at varying distances from the injection port (0 to 38 mm, 38 to 76 mm, 76 to 114 mm, and 114 to 152 mm) that were homogenized to yield representative subsamples for $CaCO_3$ content measurements. $CaCO_3$ contents were quantified in accordance with ASTM D4373 (ASTM, 2014) by reacting $CaCO_3$ in soil samples with 1 M hydrochloric acid to generate CO_2 gas and a corresponding increase in test chamber pressure. Relationships between chamber pressure and known reagent-grade $CaCO_3$ masses were used to determine sample $CaCO_3$ contents. A minimum of three $CaCO_3$ content measurements were completed per column section and all section values were averaged to determine average $CaCO_3$ contents for columns.

2.8. Previous meter-scale soil column experiments

Results from past meter-scale experiments by San Pablo et al. (2020) are discussed to compare results obtained from reactive transport simulations performed in this study to past observations from physical experiments. Although more details regarding these experiments can be found in San Pablo et al. (2020), a brief summary of relevant details is provided here. Two 3.67-m-long soil column experiments containing Concrete Sand were treated to achieve relatively low and high ureolytic reaction rates to examine the effect of microbial activity on achieved cementation magnitudes and uniformity. All columns received 6 stimulation and 9 cementation injections that were 1.5 PV in volume and were applied at a constant injection rate (0.48 PV/h). Prior to all injections, passive tracer tests were performed to determine column advective-dispersive transport properties. Passive tracer testing involved the injection of 76 L (1.5 PV) of a 15 mM NaBr solution followed by 76 L (1.5 PV) of deionized water with samples collected at the column outlet. Bromide ion (Br^-) concentrations in samples were assessed using solution conductivity measurements and breakthrough curves were determined. Ureolytic rates were monitored during the 9th cementation treatment using samples obtained from four ports along the length of the columns. Soil $CaCO_3$ contents were also quantified along column lengths after treatments.

2.9. PHREEQC modeling

A one-dimensional advective-dispersive soil column transport model was developed using the geochemical software PHREEQC (Parkhurst and Appelo, 2013) to further explore the implications of the ureolytic rates achieved in the centimeter-scale soil columns on biocementation magnitudes and distributions expected at meter-scale. Simulations allowed for changes in urea hydrolysis rates, injection rates, and their collective impacts on biocementation spatial distributions to be subsequently explored in the context of meter-scale experiments to expand understandings beyond the specific conditions investigated by San Pablo et al. (2020). Simulations investigated treatment injections applied to a column model that was identical to that tested by San Pablo et al. (2020) and was 3.67 m in length, had a square cross-sectional area of 0.04 m^2, and consisted of 163 cells (length of 0.022 m each). A passive tracer injection sequence identical to the physical experiments was simulated using the PHREEQC soil column model and the model's mobile porosity (n) and longitudinal dispersivity (α_L) values were calibrated to match experimental passive tracer data. Although each column had a physical pore volume (PV) of 50 L, an apparent PV of 37.5 L was used in the model to match passive tracer data due to the presence of air bubbles. All models had a hydraulic conductivity of 2.2×10^{-4} m/s following experimental measurements.

In all PHREEQC simulations, ureolysis was modeled as a kinetic reaction using the Michaelis-Menten ureolytic kinetic expression presented in Eq. (1) wherein K_m is the half-saturation coefficient in [mM urea] and bulk V_{max} is the maximal velocity of bulk solution in [mM urea $hour^{-1}$]. Although actual K_m values vary between stimulated ureolytic strains, the value reported by Graddy et al. (2018) for *Sporosarcina pasteurii* (ATCC 11859) (K_m = 305 mM urea) well approximated experimentally observed urea degradation trends and was used for all simulations. By varying the bulk V_{max}, the ureolytic kinetic model was calibrated to match experimentally observed urea degradation trends from centimeter-scale soil columns. In all models, $CaCO_3$ precipitation was treated as an equilibrium reaction [Eq. (2)] following recent experiments that demonstrated that $CaCO_3$ precipitation occurs exceedingly fast once CO_3^{2-} ions are produced from microbial ureolysis (Burdalski and Gomez, 2020). In all simulations, columns received a single 76 L (1.5 PV) injection of a cementation solution that was identical to that used in both experiment set B and the physical experiments by San Pablo et al., 2020 (250 mM calcium chloride, 250 mM urea, 12.5 mM NH_4Cl, and 42.5 mM sodium acetate). In order to examine changes in reactive transport conditions, injections were applied at varying injection rates ranging from 0.06 PV/h to 1.8 PV/h (50 to 1500 mL/min) and different ureolytic rates were considered, which encompassed variations observed in centimeter-scale experiments. Models were calibrated to capture three different ureolytic rates representative of the 0.01 g/L YE daily, 0.07 g/L YE alternating, and 0.2 g/L YE daily columns from experiment set A during the 8th cementation injection. In all simulations, urea hydrolysis activities were assumed to be spatially uniform along columns with length following data from San Pablo et al. (2020) which indicated that relatively similar stimulated ureolytic activities could be obtained along meter-scale injection pathways with no consistent bias in activities towards the injection or production locations.

$$\frac{d[Urea]}{dt} = \left(\frac{Bulk\ V_{max}[Urea]}{K_m + [Urea]}\right) \quad (1)$$

$$Ca^{2+} + CO_3^{2-} \rightarrow CaCO_{3\ solid} \quad \left(K_{sp} = 10^{-8.48}\right) \quad (2)$$

3. Results and discussion

3.1. Set A centimeter-scale soil column experiments

Fig. 1 presents measurements of solution urea concentrations in time for all centimeter-scale soil columns during experiment set A for three stimulation injections and four cementation injections. Although no significant urea hydrolysis activity was observed in any column during the second stimulation injection (Fig. 1a); as stimulation injections proceeded, increases in urea hydrolysis activity were observed with all columns except the 0.01 g/L YE daily column degrading more than ≈20 mM and ≈40 mM urea during stimulation injections 4 and 6, respectively (Fig. 1b, c). Increasing ureolytic rates were expected during successive injections of a selective growth medium, which stimulated the growth of ureolytic bacteria and progressively biased microbial communities towards increased ureolytic activity. During the cementation phase, solution urea concentrations increased from 50 mM to 350 mM and more significant differences in rates were observed. During cementation injection 3, the 0.2 g/L YE daily, 0.07 g/L YE daily, and the 0.07 g/L YE alternating columns hydrolyzed approximately 341 mM, 236 mM, and 106 mM urea, respectively, after only 8 h. However, no detectable urea degradation was observed in the 0.01 g/L YE daily column after the full 24-h retention period (Fig. 1d). After cementation injection 6, pseudo-steady urea hydrolysis rates were observed in all columns except the 0.01 g/L YE daily column (Fig. 1e, f, g), where urea hydrolysis rates continued to increase with further injections but remained significantly lower than other columns. When comparing urea hydrolysis rates, increases in ureolytic activity consistently corresponded to increases in applied YE concentrations (Fig. 1b to 1g) with the alternating 0.07 g/L YE column also achieving notable rate reductions when compared to the similar 0.07 g/L YE daily column.

Fig. 2 presents normalized urea degradation ($\Delta C/C_0$) observed in all set A columns during the 24-h injection and retention periods for all treatments. Normalized urea degradation was calculated by dividing the concentration of urea hydrolyzed during treatment periods (ΔC) by the initial urea concentration (C_0). As shown, limited urea degradation was observed in all columns until stimulation injection 3, during which 75% of the injected urea concentration was hydrolyzed in the 0.07 g/L YE daily column (Fig. 2a). The appearance urea hydrolysis in this column before the 0.2 g/L YE daily column was unexpected and suggested that either higher YE transiently favored certain non-ureolytic subgroups (i.e., protein-degrading clostridia) or that there was some variability in initial microbial populations between columns. However, as stimulation injections proceeded, increases in applied YE concentrations resulted in consistent increases in urea degradation magnitudes. During the last stimulation injection, between 85% and 95% of the injected urea was

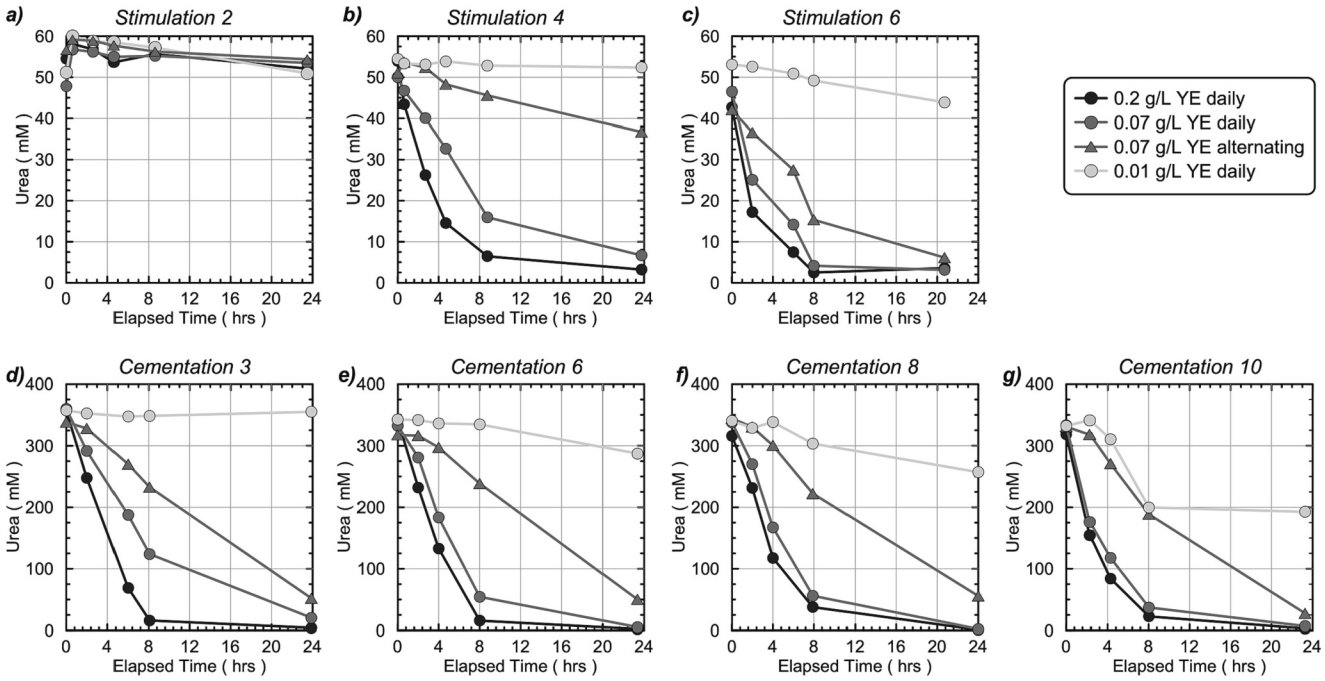

Fig. 1. Solution urea concentrations (mM) in time during the (a) 2nd, (b) 4th, and (c) 6th stimulation injection and the (d) 3rd, (e) 6th, (f) 8th, and (g) 10th cementation injection for all set A columns.

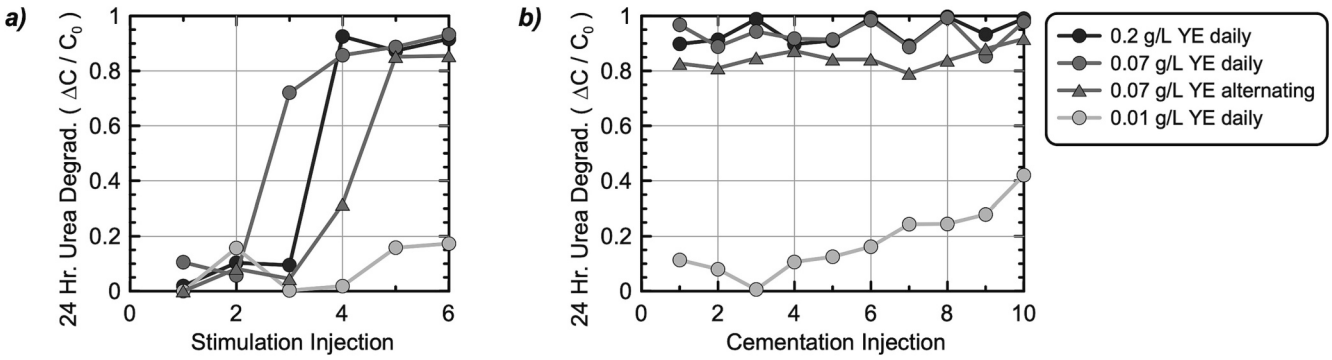

Fig. 2. Normalized urea degradation ($\Delta C/C_o$) observed after 24-h injection and retention periods during all (a) stimulation and (b) cementation injections in set A columns.

hydrolyzed after 24 h in all columns except the 0.01 g/L YE daily column which achieved only 17% degradation. While similar urea degradation magnitudes were maintained in almost all columns during cementation, urea degradation continued to increase in the 0.01 g/L YE daily column with nearly 45% of the injected urea hydrolyzed during the last cementation injection (Fig. 2b). In order to better quantify differences in ureolytic rates, changes in bulk V_{max} values were further examined by fitting the ureolytic kinetic expression [Eq. (1)] to observed urea degradation trends (Supplemental Fig. S2). Bulk V_{max} values ranged between 3 and 89 mM/h during stimulation, but increased to between 3 and 134 mM/h during cementation. Despite similar cumulative urea degradation observed during all cementation injections (Fig. 2b), bulk V_{max} values in the in the 0.2 g/L and 0.07 g/L YE daily columns continued to increase during cementation suggesting ongoing enrichment for ureolysis. In the 0.07 g/L YE alternating column, bulk V_{max} values instead remained relatively constant, however, likely due to the absence of nutrients included in alternate injections, which are speculated to have maintained near constant ureolytic cell densities. In the 0.01 g/L YE daily column, bulk V_{max} values increased slightly after cementation injection 3 but remained <12.5 mM/h.

Following cementation, $CaCO_3$ content measurements were performed for all columns. Supplemental Fig. S3 presents measured soil $CaCO_3$ contents along column lengths and Supplemental Table S2 provides all $CaCO_3$ content measurements for sections as well as average $CaCO_3$ contents for entire columns. All columns except the 0.01 g/L YE daily column achieved similar $CaCO_3$ content distributions with average $CaCO_3$ contents between 4.3 and 4.9% by mass, which was consistent with the comparable urea degradation observed during retention periods (Fig. 2b). In the 0.01 g/L YE daily column, a significantly lower average $CaCO_3$ content of 1.8% by mass was obtained due to more limited urea degradation during injections with a more pronounced $CaCO_3$ content gradient also observed, which may have been indicative of somewhat higher ureolytic activity near the injection source. Although a significant gradient in cementation was observed in the lowest ureolytic rate column, it was hypothesized that this nonuniformity primarily resulted from incomplete reactions during the retention period. It was therefore anticipated that if lower ureolytic rates were to be employed, post-injection retention periods would need to be extended accordingly to enable full utilization of the supplied urea and calcium concentrations and more uniform $CaCO_3$ contents; an aspect

that was further investigated in experiment set B.

3.2. Set B centimeter-scale soil column experiments

Fig. 3 presents measurements of solution urea concentrations in time for all centimeter-scale soil columns during experiment set B for two stimulation injections and three cementation injections. In order to allow columns with lower ureolytic rates to achieve greater reaction completion during residence periods, cementation injection retention periods were extended from 24 h (as was used in set A) to 48 h; however, stimulation injections were still applied once every 24 h. Although detectable urea degradation was only observed in the 0.2 g/L YE columns during stimulation injection 2 (Fig. 3a), significant ureolytic activity was observed in all columns during stimulation injection 6 with increases in ureolytic rates consistently corresponding to increases in supplied YE concentrations and application frequencies. At the end of stimulation, both 0.2 g/L YE columns achieved similarly high ureolytic activities, with columns receiving lower YE concentrations achieving a broader range of ureolytic rates and significant differences in rates observed between columns receiving alternating and daily YE injections (Fig. 3b). During cementation, ureolytic rates continued to accelerate in all columns (Fig. 3c to 3e) with rates becoming similar in all higher YE columns (YE $\geq$ 0.04 g/L) after cementation injections 5. Interestingly, when comparing columns that received similar total masses of YE on a differing schedule (i.e., 0.04 g/L YE daily vs. 0.08 g/L YE alternating, 0.02 g/L YE daily vs. 0.04 g/L YE alternating), similar but slightly higher rates were generally observed in the column receiving alternating higher YE injections.

Fig. 4 presents normalized urea degradation ($\Delta C/C_o$) observed 24-h after stimulation and cementation injections and 48-h after cementation injections. As shown, detectable ureolytic activity appeared to occur earlier with increases in applied YE concentrations with significant urea degradation observed in all columns after stimulation injection 5 (Fig. 4a). Immediately following the transition to cementation, similar degradation magnitudes were maintained in all higher YE columns (YE $\geq$ 0.08 g/L); however, in lower YE columns (0.04 g/L YE and 0.02 g/L YE), notable reductions in degradation magnitudes were observed (Fig. 4b). Despite some large differences in 24-h degradation between columns, almost all columns achieved full degradation of the supplied urea after 48 h during cementation, with the exception of the 0.02 g/L YE columns which achieved full degradation after cementation injection 4 (Fig. 4c). Bulk V_{max} values were also determined from urea degradation trends to examine differences in ureolytic rates with bulk V_{max} values ranging between 13 and 76 mM/h during the last stimulation injection, bulk V_{max} values decreasing in almost all columns during the initiation of cementation, followed by progressive increases in bulk V_{max} values during cementation to between 25 and 89 mM/h during the last cementation injection (Supplemental Fig. S4). Although the reduction in bulk V_{max} values immediately after the transition to cementation was unexpected due to the presence of higher urea concentrations, this outcome was similar to observations from previous studies (Gomez et al., 2018b) and may have resulted from a variety of differences including (1) cell elution from the additional flush injection applied prior to cementation, (2) large changes in solution composition and ionic strength which may have increased cell osmotic stress, and (3) the initiation of $CaCO_3$ precipitation which may have acted to encapsulate cells and reduce bulk ureolytic activity (van Paassen, 2009; Cuthbert et al., 2012).

Soil shear wave velocities were measured at mid-depth within all soil columns during cementation injections to track changes in cementation progression (Supplemental Fig. S5). All V_s values were near 80 m/s immediately prior to cementation and increased in a near-linear manner to final V_s values between 500 and 650 m/s after 9 cementation injections. Similar V_s trends for all columns in time suggested that similar engineering improvements and $CaCO_3$ magnitudes were achieved between columns at mid-depth. Supplemental Fig. S6 presents measured soil $CaCO_3$ contents along column lengths and Supplemental Table S3 summarizes final shear wave velocity increases (ΔV_s) and $CaCO_3$

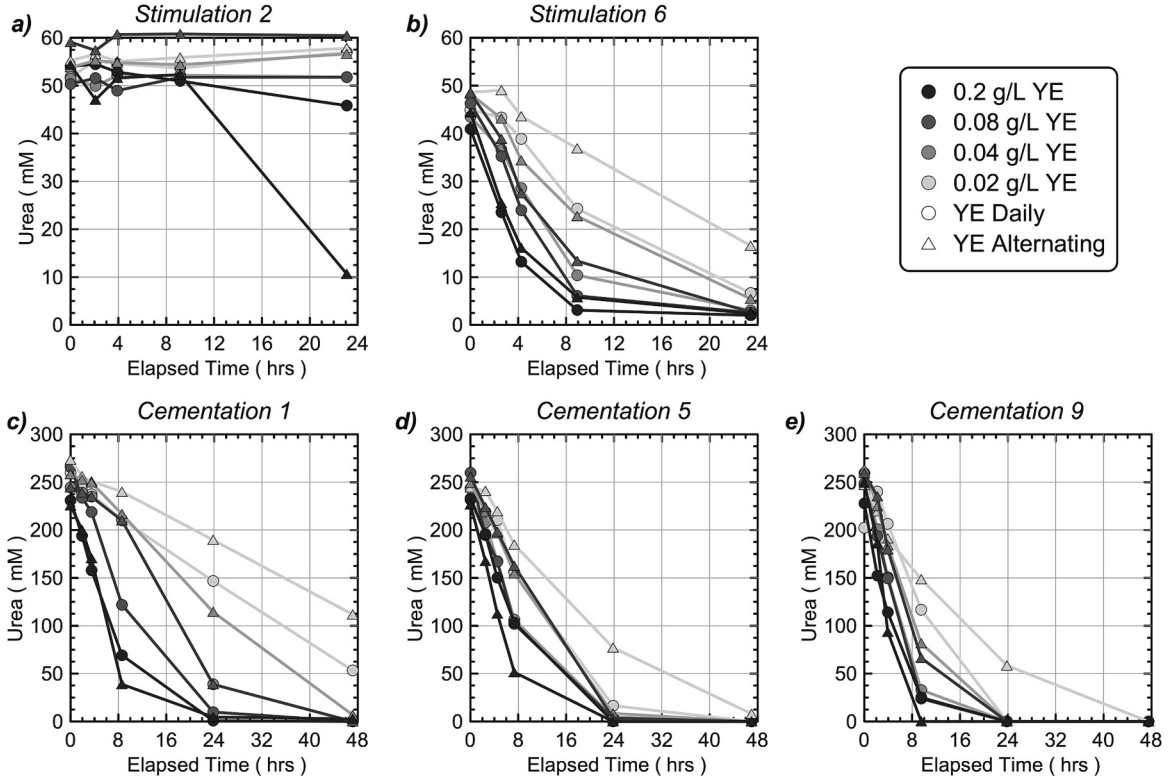

Fig. 3. Solution urea concentrations (mM) in time during the (a) 2nd and (b) 6th stimulation injection and the (c) 1st, (d) 5th, and (e) 9th cementation injection for all set B columns.

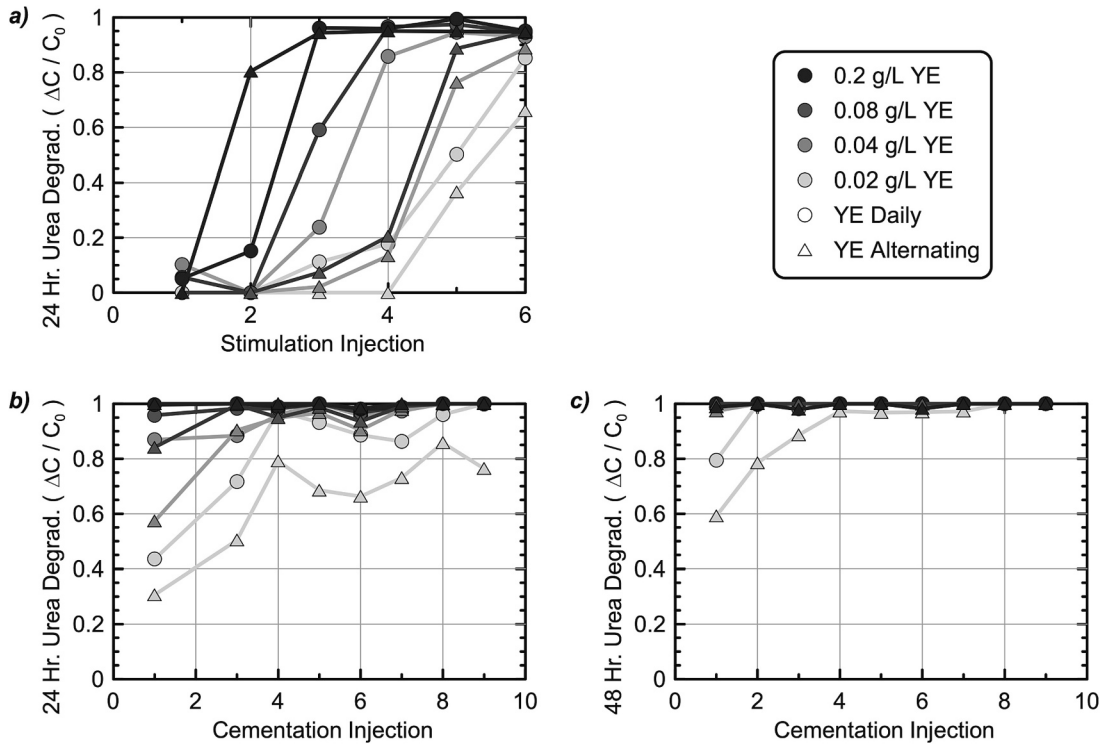

Fig. 4. Normalized urea degradation ($\Delta C/C_0$) observed 24-h after all (a) stimulation and (b) cementation injections and 48-h after all (c) cementation injections in set B columns.

content measurements for all columns including section and average $CaCO_3$ content values. All columns had similar soil $CaCO_3$ content distributions with small decreases in $CaCO_3$ contents observed with increasing distance from the injection source. For all columns, average $CaCO_3$ contents were between 3.5% and 4.4% by mass and were consistent with past column studies for similar ΔV_s values (Gomez and DeJong, 2017). No significant differences in post-treatment improvements were observed between columns as a function of supplied YE concentrations or YE treatment frequencies and outcome that was consistent with the similar 48-h urea degradation observed between all columns during cementation (Fig. 4c).

3.3. Summary of ureolytic rates obtained in centimeter-scale soil column experiments

Fig. 5 summarizes bulk V_{max} values versus supplied YE concentrations for all columns from both experimental sets to better understand how rates correlated to supplied nutrient concentrations. As shown, variations in supplied YE concentrations and YE treatment frequencies resulted in a wide spectrum of bulk V_{max} values (i.e., urea hydrolysis rates) between 3 and 89 mM/h at the end of stimulation (stimulation injection 6) which increased to between 16 and 134 mM/h during the final cementation injections. In both experiments, greater YE concentrations and YE treatment frequencies consistently resulted in higher ureolytic rates; however, YE concentrations exhibited non-linear relationships with achieved microbial activities, indicating that increases in ureolytic cell densities were not linear with increases in supplied YE. This outcome suggested that while components within YE strongly limited ureolytic cell growth at the community level, other factors such as limited dissolved oxygen, metabolic waste generation, and/or other trace nutrient requirements may have limited growth at higher YE. Furthermore, large differences in stimulated ureolytic

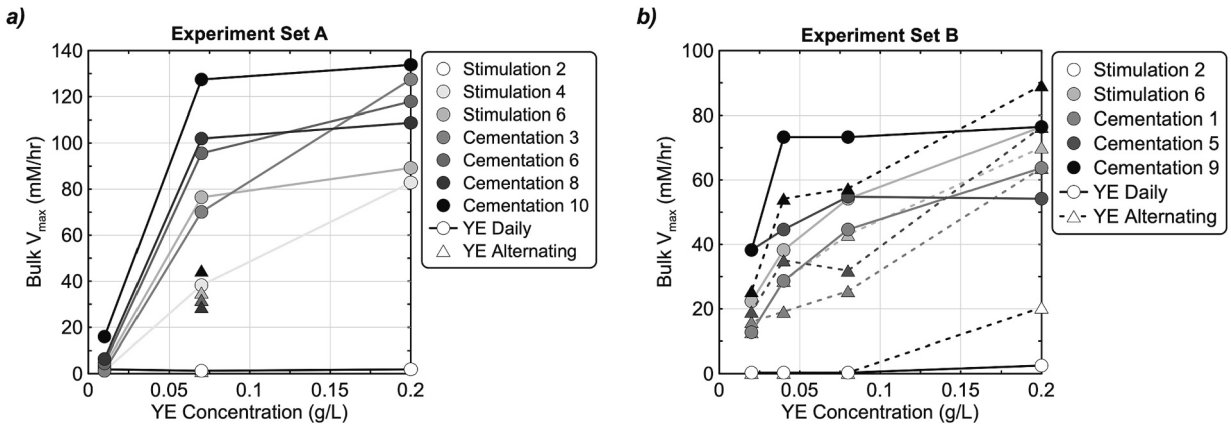

Fig. 5. Bulk V_{max} values versus supplied YE concentrations obtained during select stimulation and cementation injections for all soil columns from experiment set (a) A and (b) B.

activity as a function of supplied YE were noteworthy given the excess of acetate organic carbon in all treatment solutions (85 mM C) relative to the ≈0.8 to 17 mM C provided by YE over the range of concentrations examined (0.01 to 0.2 g/L). One interpretation is that the growth of enriched ureolytic bacteria, primarily using acetate, was limited by specific growth factors provided by YE, such as trace elements or essential vitamins, and not total organic carbon. Another potential explanation could be that while acetate supports biosynthesis, it is not a sufficient sole energy source for ureolytic bacteria, with some components of YE, such as amino acids, being essential, thus rendering it the limiting nutrient. Interestingly, when comparing achieved ureolytic rates between experimental sets at similar YE concentrations, experiment set B columns consistently exhibited lower bulk V_{max} values during cementation. This outcome likely resulted from the lower urea concentrations included in cementation solutions applied in experiment set B (250 mM) in comparison to experiment A (350 mM), which reduced post-treatment pH values and total ammonium concentrations and likely reduced selective pressure for enrichment of ureolytic bacteria. Despite rate differences between sets, almost all columns exhibited considerable ureolytic rate increases during cementation. Interestingly, columns receiving both lower YE concentrations (< 0.07 g/L) and alternating YE additions also appeared to exhibit a more linear relationship between supplied YE and achieved rates when compared to higher YE and daily YE columns, respectively. The use of lower YE concentrations and alternating YE treatment strategies may therefore allow for a desired ureolytic rate to be more easily obtained, with variations in YE provided greater latitude with respect to altering achieved rates. Alternating nutritive/non-nutritive injections also appeared to minimize rate changes throughout the treatment process when compared to daily YE columns and may be preferred for applications where near constant rates are desired. Although large differences in ureolytic rates were achieved between columns, similar post-treatment $CaCO_3$ content distributions and engineering improvements were observed for nearly all columns and suggested that when retention periods were sufficient to enable full reaction completion, lower ureolytic rates could be used to minimize reactions during injections without sacrificing process efficacy.

3.4. Reactive transport simulations

Informed by previous results from the centimeter-scale soil column experiments, twenty-seven reactive transport simulations were performed to investigate relationships between ureolytic rates, solution transport conditions, and biocementation distributions realized in 3.67-m-long soil column numerical models similar to that physically tested by San Pablo et al. (2020). In order to calibrate the PHREEQC advective-dispersive soil column numerical models to passive tracer data from the actual meter-scale experiments, simulated normalized bromide concentrations (C/C_0) were compared to experimental measurements (Supplemental Fig. S7). A mobile porosity (n) of 0.234 and longitudinal dispersivity (α_L) of 0.3 m was assumed in the model and was able to well capture normalized bromide concentrations during the passive tracer injection sequence. The numerical model allowed for the implications of the treatment techniques identified in the previous centimeter-scale soil column experiments to be applied at meter-scale under varying reactive transport conditions.

In order to explore the full spectrum of ureolytic rates realized in the previous centimeter-scale soil column experiments, the Michaelis-Menten kinetic model [Eq. (1)] was calibrated to urea degradation trends for the 0.01 g/L YE daily, 0.07 g/L YE alternating, and 0.2 g/L YE daily columns from experiment set A during cementation injection 8. Fig. 6 presents normalized urea concentrations (C/C_0) in time from the centimeter-scale columns and the calibrated PHREEQC models which assumed bulk V_{max} values of 6.4, 28.8, and 108.8 mM urea/h for the 0.01 g/L YE daily, 0.07 g/L YE alternating, and 0.2 g/L YE daily columns, respectively. After calibrating the soil column models to capture both advective-dispersive transport properties and ureolytic reaction rates, simulations were performed considering nine different injection flow rates (0.06 PV/h to 1.8 PV/h) and the three ureolytic reactions rates shown in Fig. 6. In all simulations, a single 1.5 PV cementation solution injection was applied similar to that employed in San Pablo et al. (2020) and $CaCO_3$ distributions were determined along column lengths both immediately after injections as well as following a retention period that was varied to allow for complete ureolysis and cementation reactions. Table 1 presents a summary of all PHREEQC soil column simulations including injection rates, injection volumes, injection durations, ureolytic reaction rates, post-injection reaction durations, total model durations, and reaction-to-injection duration ratios (described later).

Fig. 7 presents simulated soil column $CaCO_3$ distributions immediately after injections, representing the reactions during transport, (Fig. 7a, b, c) and after reaction completion (Fig. 7d, e, f) for three select injection rates (0.06 PV/h, 0.3 PV/h, and 1.8 PV/h) as well as the three different ureolytic rates shown in Fig. 6. At the slowest injection rate (0.06 PV/h), significantly larger $CaCO_3$ contents were observed near the injection source (distance = 0 m) both immediately after injections

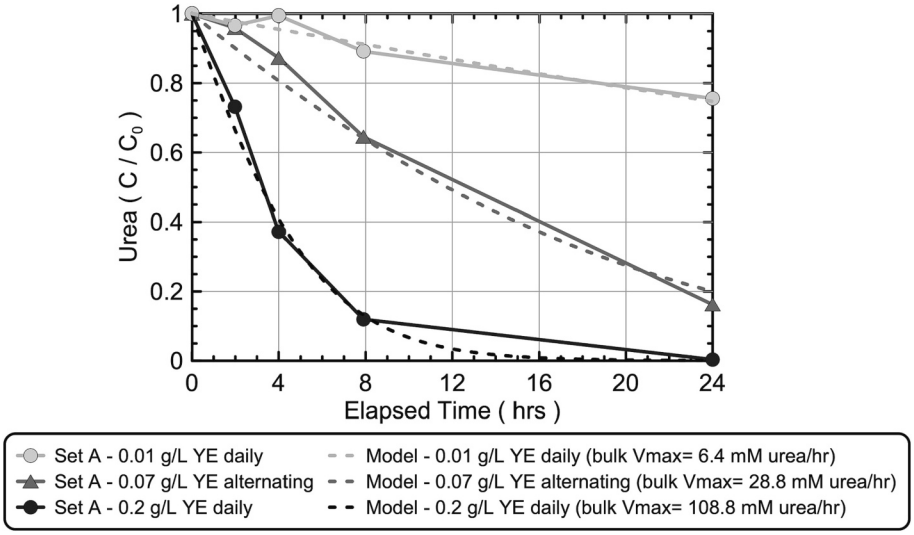

Fig. 6. Comparison of normalized urea concentrations (C/C_0) in time from the 0.01 g/L YE daily, 0.07 g/L YE alternating, and 0.2 g/L YE daily columns from set A during cementation injection 8 with simulated trends from PHREEQC models assuming bulk V_{max} values of 6.4, 28.8, or 108.8 mM urea/h.

Table 1
Summary of PHREEQC 3.67-m-long soil column simulations.

Injection rate		Injection volume	Injection duration	Ureolytic reaction rate (from experiment set A)	Post-injection reaction duration (C/C0 < 5%)	Total model duration	Reaction-to-injection duration ratio (RTIDR)
(PV/h)[1]	(mL/min)	(PV)[1]	(hr)	–	(hr)	(hr)	–
				0.2 g/L YE daily	10.7	36.0	0.4
0.06	50	1.5	25.3	0.07 g/L YE alternating	38.9	64.2	1.5
				0.01 g/L YE daily	174.6	199.9	6.9
				0.2 g/L YE daily	10.7	27.6	0.6
0.09	75	1.5	16.9	0.07 g/L YE alternating	38.9	55.8	2.3
				0.01 g/L YE daily	174.6	191.5	10.3
				0.2 g/L YE daily	10.7	23.4	0.8
0.12	100	1.5	12.7	0.07 g/L YE alternating	38.9	51.6	3.1
				0.01 g/L YE daily	174.6	187.3	13.8
				0.2 g/L YE daily	10.7	15.8	2.1
0.30	250	1.5	5.1	0.07 g/L YE alternating	38.9	44.0	7.7
				0.01 g/L YE daily	174.6	179.7	34.5
				0.2 g/L YE daily	10.7	13.2	4.2
0.60	500	1.5	2.5	0.07 g/L YE alternating	38.9	41.4	15.4
				0.01 g/L YE daily	174.6	177.1	68.9
				0.2 g/L YE daily	10.7	12.4	6.3
0.90	750	1.5	1.7	0.07 g/L YE alternating	38.9	40.6	23.0
				0.01 g/L YE daily	174.6	176.3	103.4
				0.2 g/L YE daily	10.7	12.0	8.4
1.20	1000	1.5	1.3	0.07 g/L YE alternating	38.9	40.2	30.7
				0.01 g/L YE daily	174.6	175.9	137.8
				0.2 g/L YE daily	10.7	11.7	10.6
1.50	1250	1.5	1.0	0.07 g/L YE alternating	38.9	39.9	38.4
				0.01 g/L YE daily	174.6	175.6	172.3
				0.2 g/L YE daily	10.7	11.5	12.7
1.80	1500	1.5	0.8	0.07 g/L YE alternating	38.9	39.7	46.1
				0.01 g/L YE daily	174.6	175.4	206.8

[1] 1 PV = 50 L following San Pablo et al. (2020)[48]. Note that the apparent PV of modeled columns was a smaller 37.5 L, however, due to the presence of air bubbles in the physical experiment.

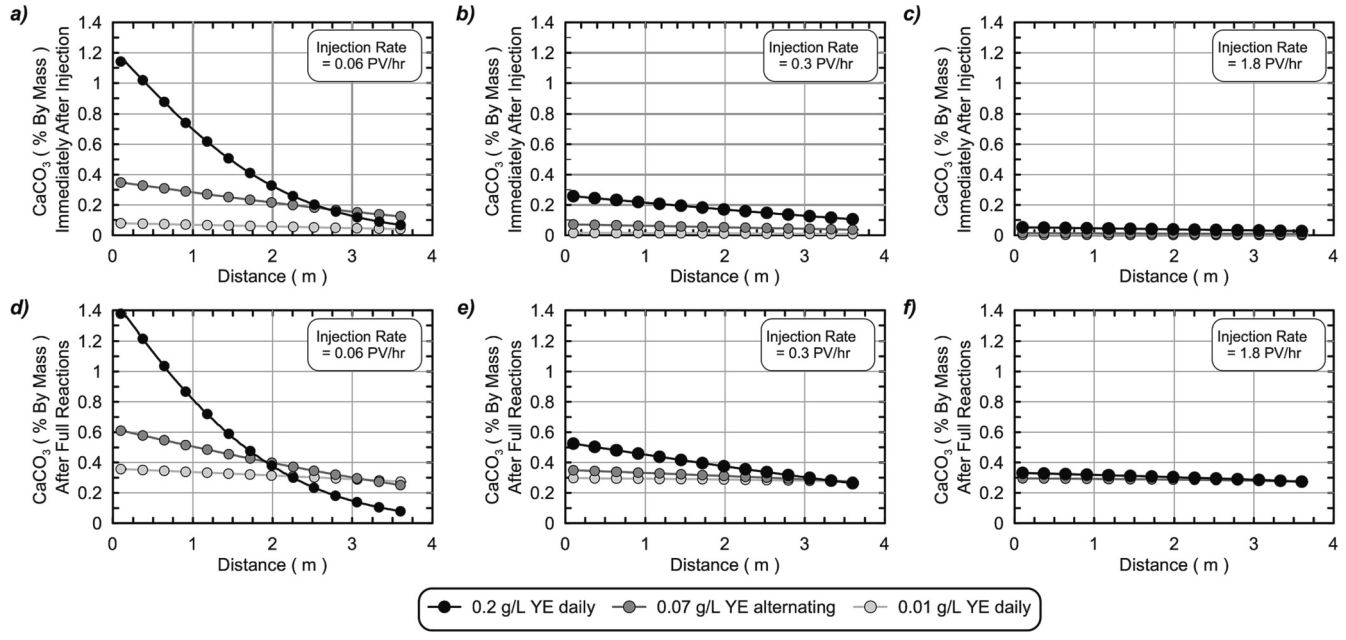

Fig. 7. Simulated soil column $CaCO_3$ distributions (a, b, c) immediately after injections and (d, e, f) following reaction completion for select injection rates including (a, d) 0.06 PV/h (50 mL/min), (b, e) 0.3 PV/h (250 mL/min) and (c, f) 1.8 PV/h (1500 mL/min) for the three different ureolytic reaction rates obtained from Fig. 9 (as described by YE additions).

(Fig. 7a) and after reaction completion (Fig. 7d) when compared to the end of the column (distance = 3.67 m). Localization of biocementation near the injection source became more pronounced with both decreases in flow rates and increases in ureolytic activities, which resulted in greater urea hydrolysis and precipitation reactions during injections thereby limiting the transport of reactants (i.e., urea, Ca^{+2}) to farther distances within columns. In contrast, as injection rates increased, more limited reactions occurred during solution transport (Fig. 7b, c) resulting in more uniform $CaCO_3$ contents along column lengths after reaction completion (Fig. 7e, f), albeit with smaller $CaCO_3$ magnitudes than those

observed for the slowest injection rate (Fig. 7d). Although the greatest localization of $CaCO_3$ near the injection source occurred in the column with the highest ureolytic rate and slowest injection rate (0.2 g/L YE daily rate, 0.06 PV/h), at this same slow injection rate, the two lower ureolytic rates (0.01 g/L YE daily, 0.07 g/L YE daily) achieved substantially improved uniformity as well as greater $CaCO_3$ contents near the end of the column (distances >2 m) (Fig. 7d). Collectively, these results demonstrated that when reactions during injections were minimized either through decreases in ureolytic rates or increases in injection rates, supplied reactants were distributed both more uniformly and over greater distances. When deployed at field-scale, such conditions may provide significant practical advantages by allowing injection and extraction wells to be installed at greater well-to-well spacings.

Differences in treatment uniformity and extent as a function of differences in ureolytic rates and injections rates were further examined between simulations using various metrics. Fig. 8 presents results from all soil column simulations including relationships between average $CaCO_3$ contents over column lengths immediately after injections (Fig. 8a) and after reaction completion (Fig. 8b), average $CaCO_3$ content increases that occurred during the residence period (calculated by taking the difference between the previous two values) (Fig. 8c), $CaCO_3$ contents observed after reaction completion at column inlets (Fig. 8d) and outlets (Fig. 8e), and the ratio between $CaCO_3$ contents at column outlets and inlets (Fig. 8f) versus injection rates. When injection rates were reduced and ureolytic rates were increased, significant increases in column average $CaCO_3$ contents were observed both immediately after injections and after reaction completion (Fig. 8a, b). This resulted from greater precipitation reactions occurring during solution transport and therefore greater utilization of the Ca^{2+} available in the provided 1.5 PV injection. As injection rates were increased above 1 PV per hour, average $CaCO_3$ contents in columns immediately after injections were nearly 0% for all ureolytic rates (Fig. 8a) with almost all $CaCO_3$ content increases occurring during retention periods (Fig. 8c). At both lower injection rates and higher reaction rates, greater precipitation was observed near the column inlet (Fig. 8d) with less precipitation near the column outlet (Fig. 8e) due to greater Ca^{2+} consumption near the injection source. Again, once injection rates exceeded 1 PV per hour, the effect of ureolytic rates on inlet and outlet $CaCO_3$ contents was minimized (Fig. 8d, e) as reactions occurring during solution injections were negligible. While changes in injection rates had significant effects on $CaCO_3$ uniformity for columns with high ureolytic rates (0.2 g/L YE daily), interestingly when lower ureolytic rates were present, the effect of injection rate on $CaCO_3$ uniformity was diminished (Figs. 8a to 8f). Moving forward, the use of lower ureolytic rates during field applications may afford reduced sensitivity of realized cementation spatial distributions to changes in solution transport rates, in addition to improvements in uniformity and extent.

$$Reaction-to-injection\ Duration\ Ratio\ (RTIDR) = \frac{Time\ to\ \frac{[Urea]}{[Urea]_{initial}} = 5\%}{Injection\ Duration} \quad (3)$$

3.5. Characterizing biocementation treatment conditions and outcomes

Results from column simulations demonstrated the combined effects of changes in injection and ureolytic rates on $CaCO_3$ precipitation magnitudes and distributions. However, in order to better characterize differences in reactive transport conditions between simulations, a dimensionless reaction-to-injection duration ratio (RTIDR) parameter was proposed which related the rate of reactions to solution transport rates. The RTIDR parameter is similar to a Damköhler number and was calculated by dividing the time required to achieve 95% hydrolysis of the supplied urea by the injection duration [Eq. (3)]. At low RTIDRs and high Damköhler number transport the time required to complete ureolysis and $CaCO_3$ precipitation reactions is small relative to the overall injection time, thus reactions occurring during injections are more significant and greater nonuniformity in produced $CaCO_3$ can be expected. In contrast, at high RTIDRs and low Damköhler number transport the reaction time is large relative to the injection time, reactions during transport are minimized, and greater uniformity in produced $CaCO_3$ can

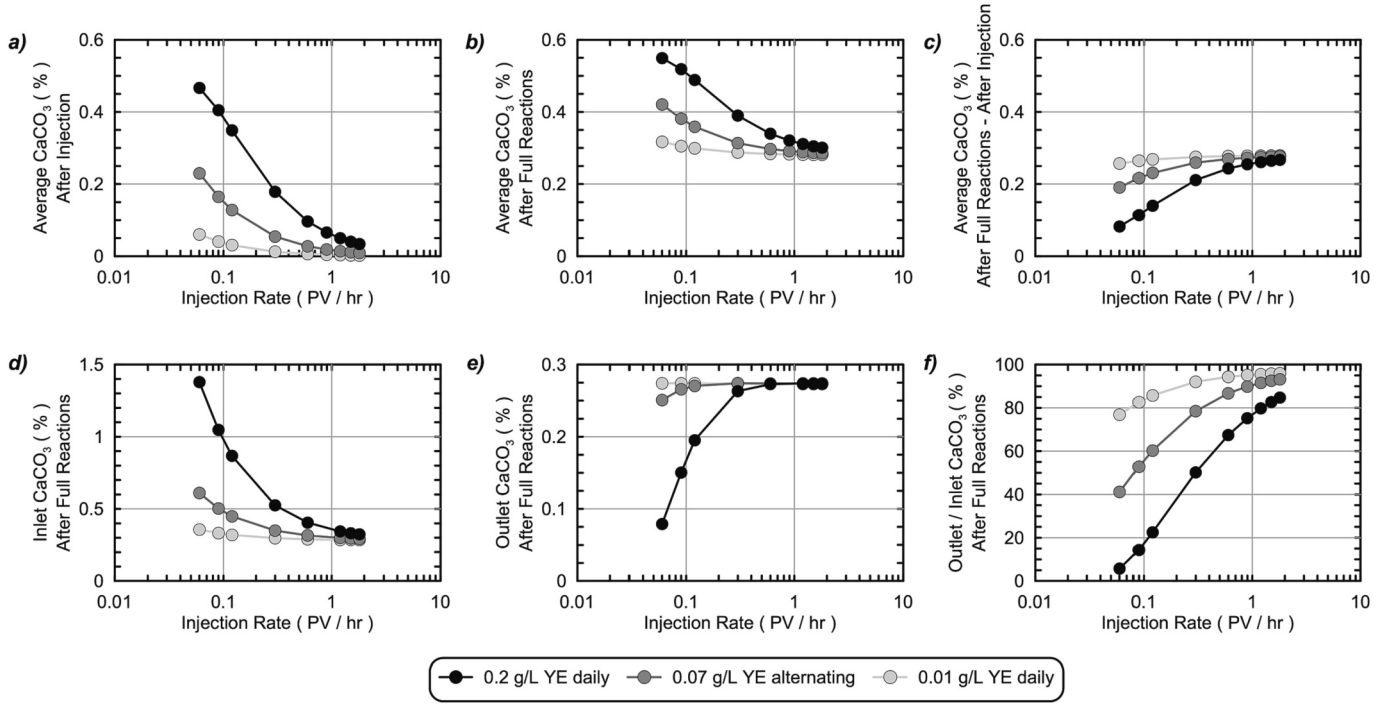

Fig. 8. Results from soil column simulations for different injection rates and ureolytic reaction rates (as described by YE additions) including: average $CaCO_3$ contents in columns (a) immediately after injections and (b) after reaction completion, (c) differences between column average $CaCO_3$ contents after injections and after reaction completion, $CaCO_3$ contents after reaction completion at the column (d) inlet and (e) outlet, and (f) outlet-to-inlet $CaCO_3$ content ratios after reaction completion versus injection rates.

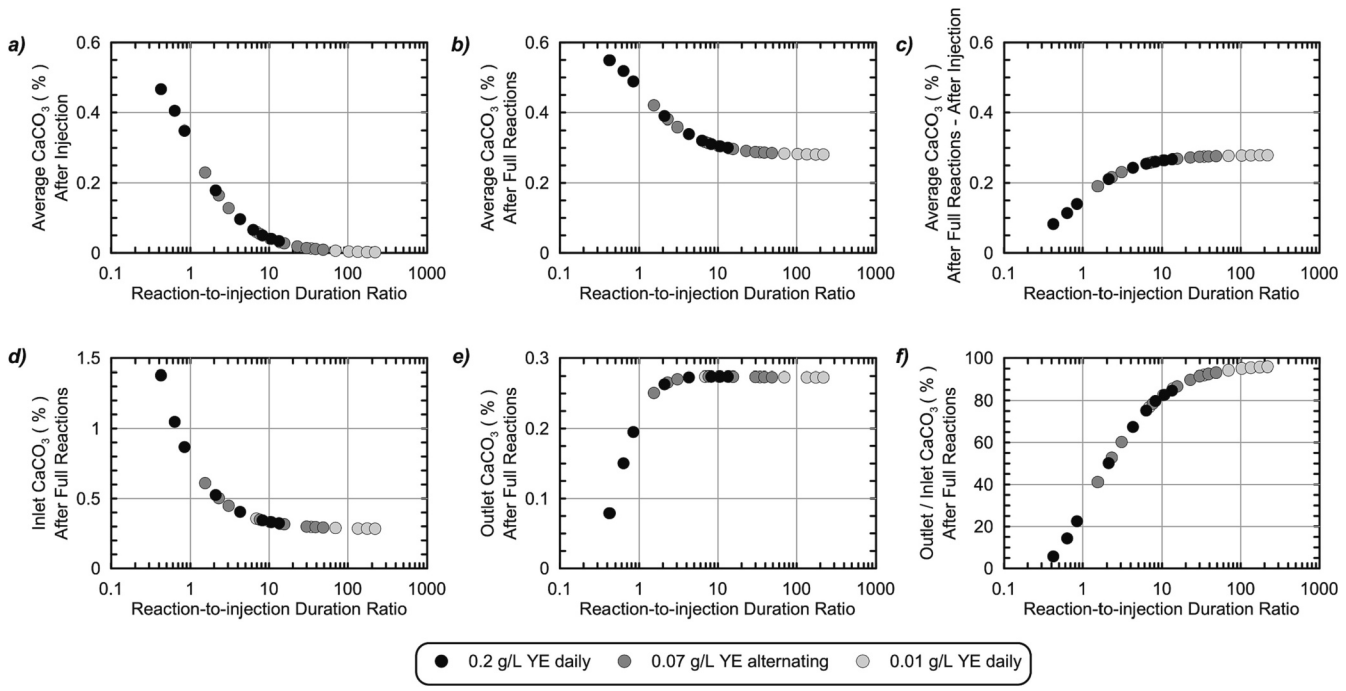

Fig. 9. Results from soil column simulations for different injection rates and ureolytic reaction rates (as described by YE additions) including: average $CaCO_3$ contents in columns (a) immediately after injections and (b) after reaction completion, (c) differences between average $CaCO_3$ contents in columns after injections and after reaction completion, $CaCO_3$ contents after reaction completion at the column (d) inlet and (e) outlet, and (f) outlet-to-inlet $CaCO_3$ content ratios after reaction completion versus dimensionless reaction-to-injection duration ratios.

be achieved. Fig. 9 presents similar parameters as Fig. 8 plotted versus the dimensionless RTIDR parameter. As shown, results from all 27 simulations were unified when plotted versus the RTIDR parameter, which reflected changes in reactive transport conditions. At RTIDR values greater than ≈10, all average, inlet, and outlet $CaCO_3$ contents were similar between simulations due to minimal reactions occurring during solution transport. At lower RTIDRs, higher average $CaCO_3$ contents were achieved (Fig. 9a and b) but at the cost of substantial nonuniformity (Fig. 9d, e, and f). Despite large differences in reaction conditions, the dimensionless RTIDR provides a unified framework for understanding the combined effects of both changes in injection and ureolytic reaction rates on biocementation distributions and magnitudes. During field-scale applications, RTIDR values may provide a valuable metric by which treatment injections can be designed to achieve desired reaction conditions and cementation distributions.

Although outlet-to-inlet $CaCO_3$ content ratios reasonably described biocementation uniformity in 1D column simulations, such ratios will not likely be suitable for assessment of treatment uniformity under field relevant flow regimes which may be complicated by the presence of three-dimensional flow, alternating injection patterns, and soil stratigraphic differences, among other factors. In order to quantitatively assess cementation uniformity and potential biases in cementation distributions towards injection or production locations, cumulative distributions of $CaCO_3$ were analyzed which describe the accumulation of cementation along an injection pathway. Cumulative distributions of $CaCO_3$ were calculated according to Eq. (4) wherein $CaCO_3$ contents were integrated with distance (X) from the injection source and normalized by the total $CaCO_3$ content integrated along the entire length of the column (L) to understand how uniformly the $CaCO_3$ was distributed with length. In this approach, a column with a fully uniform cementation distribution would exhibit a perfectly linear increase in cumulative $CaCO_3$ from 0% at the injection source to 100% at the outlet, with non-linearity in this trend being indicative of nonuniformity.

Fig. 10 presents soil $CaCO_3$ content distributions (Fig. 10a) and cumulative soil $CaCO_3$ content distributions (Fig. 10b) for column simulations with the highest (0.01 g/L YE daily, 1.8 PV/h, RTIDR = 206.8) and lowest (0.2 g/L YE daily, 0.06 PV/h, RTIDR = 0.4) reaction-to-injection duration ratios versus injection distance (Fig. 10a) and normalized injection distance (Fig. 10b). For cumulative distributions, normalized distances were computed as the distance from the injection source (X) divided by the overall length of the columns (L) to remove the influence of pathway length and generalize the approach. Similar soil $CaCO_3$ distributions are also presented for the high and low ureolytic rate meter-scale column experiments by San Pablo et al. (2020) (Fig. 10c) along with computed cumulative soil $CaCO_3$ distributions (Fig. 10d) in order to compare simulation outcomes to actual distributions realized in physical experiments. As shown, the highest RTIDR simulation (0.01 g/L YE daily, 1.8 PV/h) minimized reactions during transport and achieved a cumulative soil $CaCO_3$ content distribution with a near-constant linear slope (Fig. 10b) indicative of near complete uniformity in $CaCO_3$ along the column length (Fig. 10a). In contrast, the lowest RTIDR simulation (0.2 g/L YE daily, 0.06 PV/h) realized $CaCO_3$ contents that were much larger near the injection source resulting in a cumulative $CaCO_3$ content distribution with a concave down parabolic slope reflective of greater $CaCO_3$ masses localizing near the injection source. Results from the meter-scale column experiments by San Pablo et al. (2020) involved higher cementation magnitudes due to repeated injections, with greater cementation uniformity achieved in the low ureolytic rate column when compared to the high ureolytic rate column, despite identical flow rates (Fig. 10c). In both columns, however, greater cementation was achieved near the injection source with concave down cumulative $CaCO_3$ content distributions observed (Fig. 10d).

$$Cumulative\ CaCO_3\ Dist.(X) = \frac{\int_0^X CaCO_3\ Content}{\int_0^L CaCO_3\ Content} \times 100\% \quad (4)$$

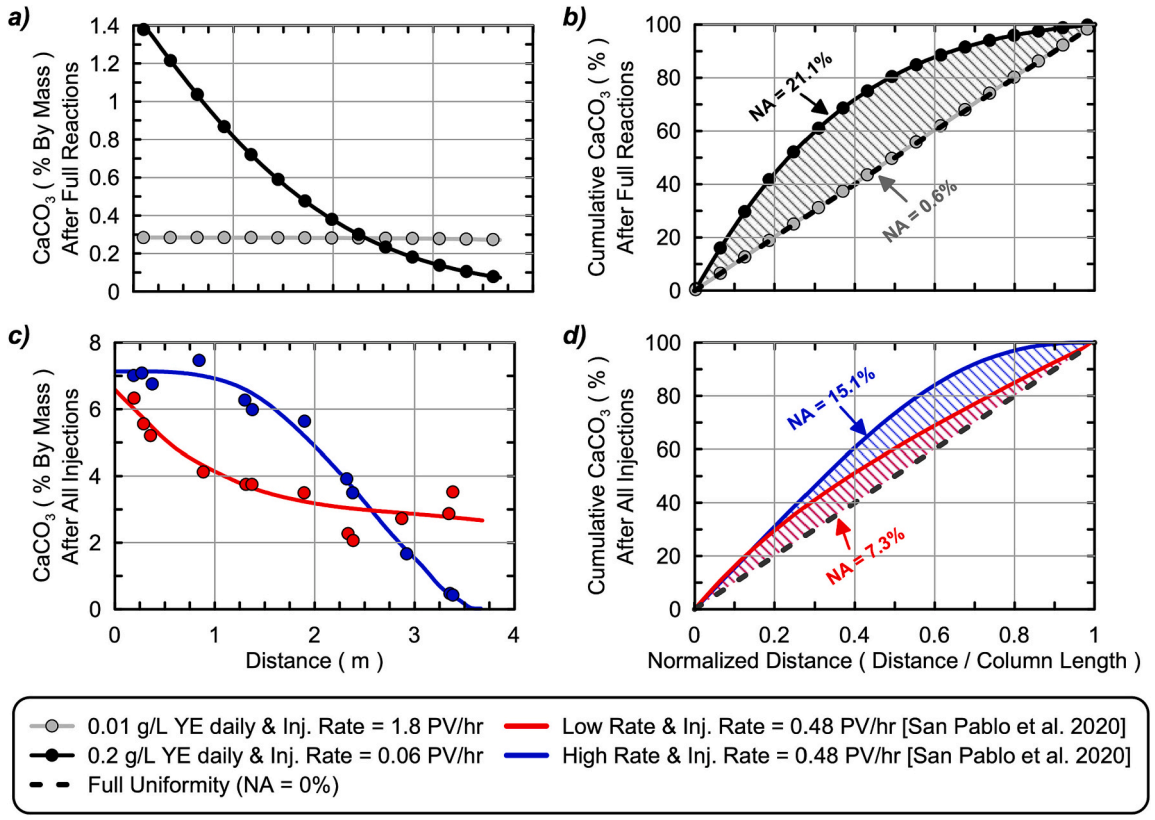

Fig. 10. (a, c) Soil column $CaCO_3$ content distributions versus distance and (b, d) cumulative $CaCO_3$ content distributions versus normalized distance for (a, b) simulations with the highest (0.01 g/L YE daily, injection rate = 1.8 PV/h) and lowest (0.2 g/L YE daily, injection rate = 0.06 PV/h) reaction-to-injection duration ratios and (c, d) low and high ureolytic rate physical meter-scale experiments by San Pablo et al. (2020) involving a constant flow rate (0.48 PV/h). Nonuniformity area (NA) values are indicated as shaded areas between respective cumulative $CaCO_3$ content distributions and dashed line trends expected for full uniformity (NA = 0%).

$$\begin{aligned} NA(\%) &= \int_{\frac{x}{L}=0}^{\frac{x}{L}=1} CumulativeCaCO_3Dist.(\%) - \int_{\frac{x}{L}=0}^{\frac{x}{L}=1} FullyUniformCumulativeCaCO_3Dist.(\%) \\ &= \int_{\frac{x}{L}=0}^{\frac{x}{L}=1} CumulativeCaCO_3Dist.(\%) - 50\% \end{aligned} \tag{5}$$

In order to quantitatively compare $CaCO_3$ content gradients between simulations and experiments irrespective of cementation magnitudes and length scales, a nonuniformity area (NA) parameter was proposed. Nonuniformity area (NA) was calculated as the area between a given cumulative soil $CaCO_3$ distribution and the cumulative soil $CaCO_3$ distribution that would be obtained for a pathway that had fully uniform cementation [Eq. (5)]. NA values are illustrated in Figs. 10b and 10d along with linear dashed lines, which represent the cumulative soil $CaCO_3$ content distributions expected for a fully uniform cemented column. NA values describe both the degree to which soil $CaCO_3$ content distributions deviate from perfect uniformity as well as the bias of the $CaCO_3$ content distributions towards the injection or production location. A positive nonuniformity area suggests that the $CaCO_3$ distribution is weighted towards the injection source and a negative nonuniformity area suggests that the $CaCO_3$ content distribution is biased towards the production location. As shown in Fig. 10, NA values were positive for both simulations indicating biases in cementation towards the injections source, with near perfect uniformity achieved in the lowest RTIDR simulation (NA = 0.6%) and more significant nonuniformity in the highest RTIDR simulation (NA = 21.1%). In the physical experiments, a similar bias in cementation was observed towards the injection source, with the low ureolytic rate column achieving a significantly lower NA (NA = 7.3%) than the high ureolytic rate column (NA = 15.1%), indicating that greater uniformity was again achieved through reductions in ureolytic rates. The ability of the NA parameter to quantify uniformity differences between the meter-scale physical experiments was particularly noteworthy given the more irregular changes in measured soil $CaCO_3$ contents with length.

Fig. 11 presents calculated NA parameters for all column simulations as well as the low and high ureolytic rate meter-scale experiments versus RTIDRs (Fig. 11a) and outlet-to-inlet $CaCO_3$ content ratios (Fig. 11b). RTIDR values for the meter-scale physical experiments were determined by fitting the ureolytic kinetic [Eq. (1)] to urea degradation trends observed from 4 sampling port locations along the length of columns during the last cementation injection and determining an average time to 95% completion of urea hydrolysis. As shown, at lower RTIDRs and

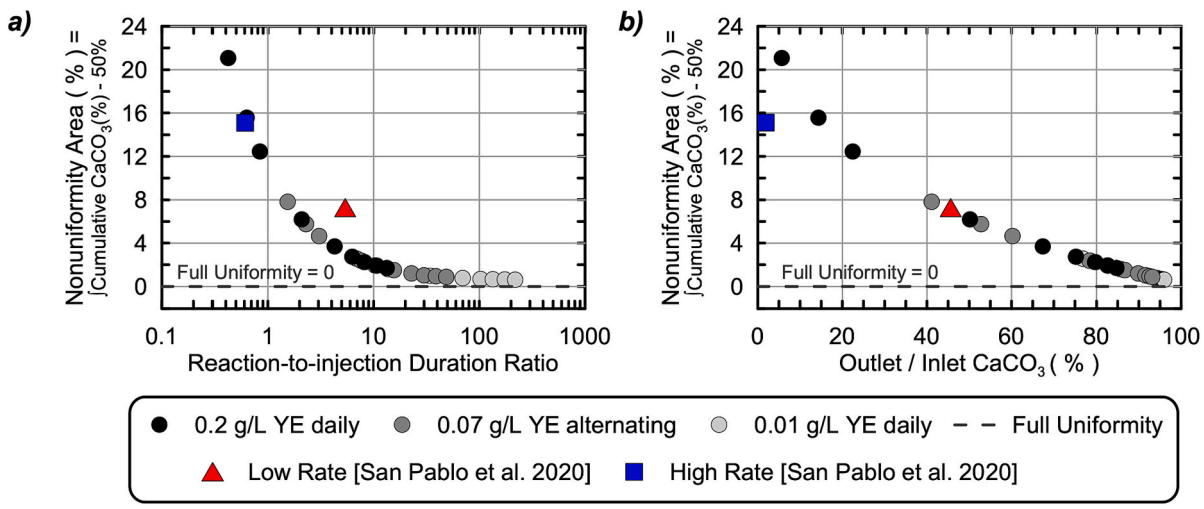

Fig. 11. Nonuniformity area parameters determined from cumulative $CaCO_3$ distributions for all soil column simulations and low and high ureolytic rate physical meter-scale experiments by San Pablo et al. (2020) versus (a) reaction-to-injection duration ratios and (b) outlet-to-inlet $CaCO_3$ ratios.

outlet-to-inlet $CaCO_3$ content ratios, large positive NA values were computed for all simulations suggesting a more significant bias of $CaCO_3$ masses towards the injection source. At higher RTIDRs and outlet-to-inlet $CaCO_3$ content ratios approaching 1, NA values decreased and approached 0%, indicative of near perfect uniformity in achieved cementation. NA values from both meter-scale physical column experiments were consistent with trends from the numerical models, suggesting that the RTIDR parameter could successfully account for differences in reaction conditions and anticipate changes in cementation nonuniformity independent of differences in injection numbers, $CaCO_3$ content magnitudes, injection rates, and ureolytic rates. As expected, outlet-to-inlet $CaCO_3$ content ratios were also well correlated with NA values for both simulations and experiments due to the application of injections in a single direction, however, the presence of more complicated injection conditions relevant to field applications (e.g., reversed injections, radial flow) may make these simplified ratios less useful for practical applications. Moving forward, the proposed NA and RTIDR parameters may allow for improved comparisons and unification of experimental observations between studies as well as allow for treatment strategies to be more effectively designed to meet site-specific engineering performance objectives (e.g., localization of cementation vs. cementation uniformity).

3.6. Practical implications of reduced reaction rates

Although all simulations considered a finite soil column length of 3.67 m, under free-field conditions more representative of field-scale applications, the applied 1.5 PV injection would have transported reagents to more distal locations beyond the column length. In order to explore anticipated effects at greater treatment distances, models were extended to 15 m in length while still applying 1.5 PV cementation solution injections under identical flow rates and reaction rates as those considered earlier. Fig. 12 presents results from 15-m-long column simulations including the percentage of supplied calcium that was precipitated within the 3.67-m length previously considered (Fig. 12a) and the maximum injection distances over which soil $CaCO_3$ contents exceeded 0.25% (Fig. 12b) and 0.1% (Fig. 12c) by mass versus RTIDR. At RTIDRs of <1, over 80% of the injected calcium was precipitated within the 3.67-m column length (Fig. 12a). As RTIDRs increased to values above 10, however, the percentage of supplied calcium that was precipitated within the column length approached 50%, which was reflective of the minimal reactions that occurred during injections. While low RTIDRs achieved greater $CaCO_3$ contents near the injection source, such conditions also resulted in a more limited extent of improvement. For example, while high RTIDR simulations (RTIDR >10) achieved $CaCO_3$ contents exceeding 0.1% at distances up to 8 m, the lowest RTIDR simulation (RTIDR = 0.4) achieved this same $CaCO_3$ content only up to 3.5 m. High RTIDR conditions may permit significant increases in treatment extent when applied under free-field conditions, with the potential to realize large reductions in process impacts and implementation costs through increased well-to-well spacings.

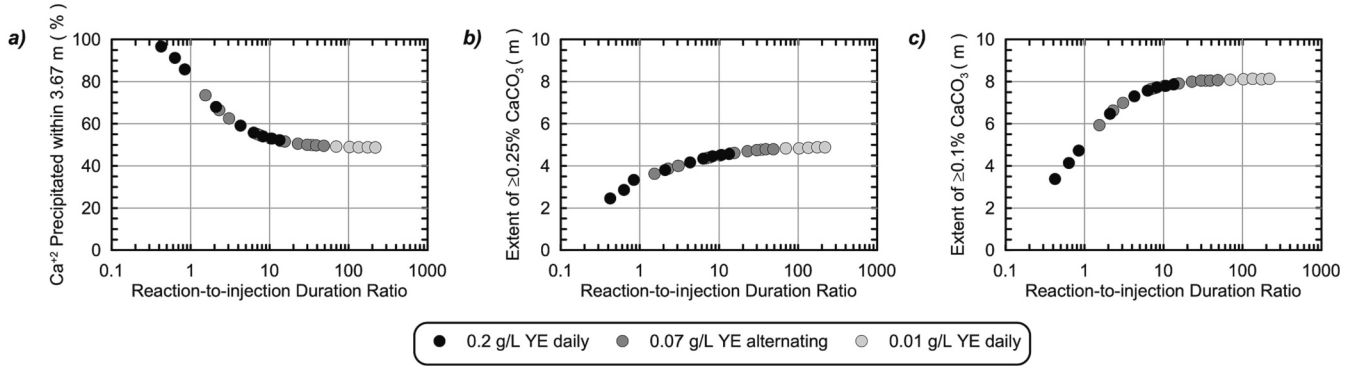

Fig. 12. Results from extended 15-m-long soil column simulations including: (a) the percentage of supplied Ca^{2+} that was precipitated within the 3.67-m-long column previously considered, and the treatment distances over which $CaCO_3$ contents exceeded (b) 0.25% and (c) 0.1% by mass versus reaction-to-injection duration ratios.

4. Conclusions

A study was completed to identify treatment approaches which could reliably enrich indigenous ureolytic microorganisms at controlled ureolytic rates to improve the spatial control of biocementation soil improvement. Twelve centimeter-scale soil column experiments were performed wherein columns received treatment solutions with varying YE concentrations intended to control enriched ureolytic cell densities and ureolytic rates. Following centimeter-scale soil column experiments, a one-dimensional reactive transport model was used to further investigate the implications of the experimentally observed ureolytic rates on the uniformity and distribution of biocementation expected in a 3.67-m-long soil column, thereby extending our understanding of changes in reactive transport conditions beyond those experimentally examined by San Pablo et al. (2020). Results from simulations were compared to those obtained from the physical meter-scale experiments and parameters to assess reactive transport conditions and cementation uniformity were explored. From the results of this study, the following conclusions can be made:

- YE concentrations supplied in MICP treatment solutions can be used to reliably control stimulated indigenous ureolytic microorganisms and achieve a wide spectrum of ureolytic rates. Ureolytic rates can be used to control reactive transport conditions during MICP and can be tailored to specific engineering applications through changes in treatment solution design.
- The ability of applied YE concentrations to reliably control stimulated ureolytic activity in the presence of significant acetate suggests that either: (1) enriched ureolytic bacteria were able to utilize the total organic carbon provided by acetate but were limited by specific growth factors provided by YE or (2) acetate was not a favorable energy source and only components of YE, such as amino acids, were utilized by ureolytic bacteria for this purpose. Applied YE concentrations had a non-linear relationship with achieved microbial activities over the range of concentrations studied suggesting that while YE strongly influenced ureolytic cell activity, other factors were limiting at high YE concentrations.
- When injection retention periods were extended to allow for full hydrolysis of the supplied urea concentrations, all centimeter-scale soil column experiments achieved similar post-treatment engineering improvements independent of differences in ureolytic activities.
- Reactive transport simulations investigated relationships between the ureolytic rates achieved in the centimeter-scale soil columns and improvement distributions expected in 3.67-m-long columns subjected to varying flow rates. Simulations demonstrated that lower ureolytic rates could achieve more uniform transport of reactants, reduced sensitivity to changes in solution injection velocities, and greater improvement extent. A reaction-to-injection duration ratio (RTIDR) parameter was shown to capture the collective impacts of changes in injection rates and ureolytic reaction rates on reactive transport conditions thereby unifying results between simulations.
- In simulations involving low reaction-to-injection duration ratios (high Damköhler number conditions), significant reactions occurred during injections, resulting in localization of cementation near injection sources, a more limited extent of improvement, and greater spatial nonuniformity. At higher reaction-to-injection duration ratios (low Damköhler number conditions), reactions occurring during transport were minimized, resulting in more uniform $CaCO_3$ distributions and a greater extent of improvement.
- A nonuniformity area (NA) parameter was introduced to quantitatively characterize changes in biocementation uniformity independent of column length and $CaCO_3$ content magnitudes for all simulations and two recent meter-scale experiments. NA provides a metric by which cementation uniformity can be quantitively assessed and compared between studies.
- Results from recent meter-scale soil column experiments by San Pablo et al. (2020) were consistent with simulated trends when both differences in injection rates and reaction rates were accounted for. Outcomes from this study further demonstrated the utility of changes in stimulated ureolytic activities to control the spatial uniformity and extent of biocementation over meter-scale treatment distances for conditions which had not yet been experimentally examined.

Although not exhaustive, the treatment techniques and reactive transport metrics identified in this study are anticipated to have important implications towards informing future MICP treatment designs and controlling the spatial distributions of ureolytic MICP for practical field-scale applications. More specifically, the study has shown that: (1) RTIDRs can be used to design treatment injections to achieve desired reaction conditions and cementation distributions with lower RTIDRs ($\langle 10$) indicating expected increases in reactions during transport and more localized improvement near an injection source and higher RTIDRs (> 10) indicating more limited reactions during transport and the potential to achieve more uniform and diffuse improvement from an injection source, (2) when stimulated MICP is employed solution YE concentrations and application frequencies can be varied to control ureolytic reaction rates with variations in YE between 0.01 and 0.07 g/L and alternating YE treatment strategies providing the greatest ability to obtain large differences in stimulated ureolytic reaction rates, (3) the nonuniformity area parameter can allow cementation uniformity to be quantitively compared between simulations, experiments, and field applications thereby allowing the success of process deployments to be assessed and verified, and (4) the use of lower stimulated ureolytic reaction rates can afford reduced sensitivity of final cementation distributions to changes in injection rates, improvements in treatment uniformity and treatment extent, increases in injection well spacings, and the potential for significant reductions in associated treatment application costs and environmental impacts.

CRediT authorship contribution statement

Minyong Lee: Conceptualization, Methodology, Formal analysis, Investigation, Resources, Writing – original draft, Writing – review & editing, Visualization. **Michael G. Gomez:** Conceptualization, Methodology, Software, Formal analysis, Investigation, Resources, Writing – original draft, Writing – review & editing, Visualization, Data curation, Supervision, Project administration, Funding acquisition. **Charles M.R. Graddy:** Conceptualization, Writing – review & editing. **Alexandra C. M. San Pablo:** Conceptualization, Writing – review & editing. **Jason T. DeJong:** Conceptualization, Writing – review & editing, Project administration, Funding acquisition. **Douglas C. Nelson:** Conceptualization, Writing – review & editing.

Declaration of Competing Interest

The authors declare the following financial interests/personal relationships which may be considered as potential competing interests:

All Authors reports financial support was provided by National Science Foundation.

Data availability

The datasets generated during and analyzed during the current study are available from the corresponding author on reasonable request.

Acknowledgments

The presented study involves work supported by the Engineering Research Center Program of the National Science Foundation (NSF) under NSF Cooperative Agreement No. EEC-1449501, NSF Award ECI-1824647, and the University of Washington. Any opinions, findings and

conclusions or recommendations expressed in this manuscript are those of the authors and do not necessarily reflect the views of the National Science Foundation. Research assistance from Colin Kolbus, Lucas Lindberg, Carson Valente, and Tyler Wilcox of the UW Biogeotechnics Lab are acknowledged and greatly appreciated.

Appendix A. Supplementary data

Supplementary data to this article can be found online at https://doi.org/10.1016/j.enggeo.2023.107104.

References

ASTM, 2014. Standard test method for rapid determination of carbonate content of soils. In: ASTM D4373-14, West Conshohocken, PA.

ASTM, 2017. Standard Practice for Classification of Soils for Engineering Purpose. ASTM D2487-17e1, West Conshohocken, PA.

Burbank, M.B., Weaver, T.J., Green, T.L., Williams, B.C., Crawford, R.L., 2011. Precipitation of calcite by indigenous microorganisms to strengthen liquefiable soils. Geomicrobiol J. 28 (4), 301–312. https://doi.org/10.1080/01490451.2010.499929.

Burbank, M., Weaver, T., Lewis, R., Williams, T., Williams, B., Crawford, R., 2013. Geotechnical tests of sands following bioinduced calcite precipitation catalyzed by indigenous bacteria. J. Geotech. Geoenviron. 139 (6), 928–936. https://doi.org/10.1061/(ASCE)GT.1943-5606.0000781.

Burdalski, R.J., Gomez, M.G., 2020. Investigating the effect of microbial activity and chemical concentrations on the mineralogy and morphology of ureolytic bio-cementation. Geo-Congress 2020, 83–95. https://doi.org/10.1061/9780784482834.010.

Cardoso, R., Pedreira, R., Duarte, S.O.D., Monteiro, G.A., 2020. About calcium carbonate precipitation on sand biocementation. Eng. Geol. 271, 105612 https://doi.org/10.1016/j.enggeo.2020.105612.

Cheng, L., Shahin, M.A., Chu, J., 2019. Soil bio-cementation using a new one-phase low-pH injection method. Acta Geotech. 14 (3), 615–626. https://doi.org/10.1007/s11440-018-0738-2.

Clarà Saracho, A., Haigh, S.K., Ehsan Jorat, M., 2021. Flume study on the effects of microbial induced calcium carbonate precipitation (MICP) on the erosional behaviour of fine sand. Géotechnique 71 (12), 1135–1149. https://doi.org/10.1680/jgeot.19.P.350.

Cuthbert, M.O., Riley, M.S., Handley-Sidhu, S., Renshaw, J.C., Tobler, D.J., Phoenix, V. R., Mackay, R., 2012. Controls on the rate of ureolysis and the morphology of carbonate precipitated by *S. Pasteurii* biofilms and limits due to bacterial encapsulation. Ecol. Eng. 41, 32–40.

Cuthbert, M.O., McMillan, L.A., Handley-Sidhu, S., Riley, Michael S., Tobler, D.J., Phoenix Vernon, R., 2013. A field and modeling study of fractured rock permeability reduction using microbially induced calcite precipitation. Environ. Sci. Technol. 47 (23), 13637–13643. https://doi.org/10.1021/es402601g.

Darby, K.M., Hernandez, G.L., DeJong, J.T., Boulanger, R.W., Gomez, M.G., Wilson, D. W., 2019. Centrifuge model testing of liquefaction mitigation via microbially induced calcite precipitation. J. Geotech. Geoenviron. 145 (10), 04019084. https://doi.org/10.1061/(ASCE)GT.1943-5606.0002122.

DeJong, J.T., Kavazanjian, E., 2019. Bio-mediated and bio-inspired geotechnics. In: Lu, N., Mitchell, J.K. (Eds.), Geotechnical Fundamentals for Addressing New World Challenges. Springer International Publishing, pp. 193–207. https://doi.org/10.1007/978-3-030-06249-1_7.

DeJong, J.T., Fritzges, M.B., Nüsslein, K., 2006. Microbially induced cementation to control sand response to undrained shear. J. Geotech. Geoenviron. 132 (11), 1381–1392. https://doi.org/10.1061/(ASCE)1090-0241(2006)132:11(1381).

DeJong, J.T., Mortensen, B.M., Martinez, B.C., Nelson, D.C., 2010. Bio-mediated soil improvement. Ecol. Eng. 36 (2), 197–210. https://doi.org/10.1016/j.ecoleng.2008.12.029.

DeJong, J.T., Soga, K.S., Kavazanjian, E., Burns, S., van Paassen, L., Al Qabany, A., Aydilek, A., Bang, S.S., Burbank, M., Caslake, L., Chen, C.Y., Cheng, X., Chu, J., Ciurli, S., Fauriel, S., Filet, A.E., Hamdan, N., Hata, T., Inagaki, Y., Jefferis, S., Kuo, M., Laloui, L., Larrahondo, J., Manning, D.A.C., Martinez, B., Montoya, B.M., Nelson, D.C., Palomino, A., Renforth, P., Santamarina, J.C., Seagren, E.A., Tanyu, B., Tsesarsky, M., Weaver, T., 2013. Biogeochemical processes and geotechnical applications: progress, opportunities and challenges. Geotechnique 63 (4), 287–301. https://doi.org/10.1680/bcmpge.60531.014.

DeJong, J.T., Gomez, M.G., San Pablo, A.C., Graddy, C.M.R., Nelson, D.C., Lee, M., Ziotopoulou, K., Montoya, B., Kwon, T.H., 2022. State of the Art: MICP soil improvement and its application to liquefaction hazard mitigation. In: Proceedings of the 20th International Conference on Soil Mechanics and Geotechnical Engineering, Sydney 2022, p. 105.

Feng, K., Montoya, B.M., 2016. Influence of confinement and cementation level on the behavior of microbial-induced calcite precipitated sands under monotonic drained loading. J. Geotech. Geoenviron. 142 (1), 04015057. https://doi.org/10.1061/(ASCE)GT.1943-5606.0001379.

Ferris, F.G., Stehmeier, L.G., Kantzas, A., Mourits, F.M., 1997. Bacteriogenic mineral plugging. J. Can. Pet. Technol. 36 (09) https://doi.org/10.2118/97-09-07.

Fujita, Y., Ferris, F.G., Lawson, R.D., Colwell, F.S., Smith, R.W., 2000. Subscribed content calcium carbonate precipitation by ureolytic subsurface bacteria. Geomicrobiol J. 17 (4), 305–318. https://doi.org/10.1080/782198884.

Fujita, Y., Taylor, J.L., Gresham, T.L.T., Delwiche, M.E., Colwell, F.S., McLing, T.L., Petzke, L.M., Smith, R.W., 2008. Stimulation of microbial urea hydrolysis in groundwater to enhance calcite precipitation. Environ. Sci. Technol. 42 (8), 3025–3032. https://doi.org/10.1021/es702643g.

Gat, D., Tsesarsky, M., Wahanon, A., Ronen, Z., 2014. Ureolysis and MICP with model and native bacteria: implications for treatment strategies. In: Geo-Congress 2014 Technical Papers, pp. 1713–1720. https://doi.org/10.1061/9780784413272.168.

Gat, D., Ronen, Z., Tsesarsky, M., 2016. Soil bacteria population dynamics following stimulation for ureolytic microbial-induced $CaCO_3$ precipitation. Environ. Sci. Technol. 50 (2), 616–624. https://doi.org/10.1021/acs.est.5b04033.

Ghasemi, P., Montoya, B.M., 2020. Field application of the microbially induced calcium carbonate precipitation on a coastal sandy slope. Geo-Congress 2020, 141–149. https://doi.org/10.1061/9780784482834.016.

Ginn, T.R., Wood, B.D., Nelson, K.E., Scheibe, T.D., Murphy, E.M., Clement, T.P., 2002. Processes in microbial transport in the natural subsurface. Adv. Water Resour. 25 (8–12), 1017–1042. https://doi.org/10.1016/S0309-1708(02)00046-5.

Gomez, M.G., DeJong, J.T., 2017. Engineering properties of bio-cementation improved sandy soils. Grouting 2017, 23–33. https://doi.org/10.1061/9780784480793.003.

Gomez, M.G., Anderson, C.M., DeJong, J.T., Nelson, D.C., Lau, X.H., 2014. Stimulating in situ soil bacteria for bio-cementation of sands. In: Geo-Congress 2014 Technical Papers, pp. 1674–1682. https://doi.org/10.1061/9780784413272.164.

Gomez, M.G., Martinez, B.C., DeJong, J.T., Hunt, C.E., deVlaming, L.A., Major, D.W., Dworatzek, S.M., 2015. Field-scale bio-cementation tests to improve sands. Proc. Inst. Civ. Eng. Ground Improvem. 168 (3), 206–216. https://doi.org/10.1680/grim.13.00052.

Gomez, M.G., Anderson, C.M., Graddy, C.M.R., DeJong, J.T., Nelson, D.C., Ginn, T.R., 2017. Large-scale comparison of bioaugmentation and biostimulation approaches for biocementation of sands. J. Geotech. Geoenviron. 143 (5), 04016124. https://doi.org/10.1061/(ASCE)GT.1943-5606.0001640.

Gomez, M.G., DeJong, J.T., Anderson, C.M., 2018a. Effect of bio-cementation on geophysical and cone penetration measurements in sands. Can. Geotech. J. 55 (11), 1632–1646. https://doi.org/10.1139/cgj-2017-0253.

Gomez, M.G., Graddy, C.M.R., DeJong, J.T., Nelson, D.C., Tsesarsky, M., 2018b. Stimulation of native microorganisms for biocementation in samples recovered from field-scale treatment depths. J. Geotech. Geoenviron. 144 (1), 04017098. https://doi.org/10.1061/(ASCE)GT.1943-5606.0001804.

Gomez, M.G., Graddy, C.M.R., DeJong, J.T., Nelson, D.C., 2019. Biogeochemical changes during bio-cementation mediated by stimulated and augmented ureolytic microorganisms. Sci. Rep. 9 (1), 11517. https://doi.org/10.1038/s41598-019-47973-0.

Graddy, C.M.R., Gomez, M.G., Kline, L.M., Morrill, S.R., DeJong, J.T., Nelson, D.C., 2018. Diversity of *Sporosarcina* -like bacterial strains obtained from meter-scale augmented and stimulated biocementation experiments. Environ. Sci. Technol. 52 (7), 3997–4005. https://doi.org/10.1021/acs.est.7b04271.

Graddy, C.M.R., Gomez, M.G., DeJong, J.T., Nelson, D.C., 2021. Native bacterial community convergence in augmented and stimulated ureolytic MICP biocementation. Environ. Sci. Technol. 55 (15), 10784–10793. https://doi.org/10.1021/acs.est.1c01520.

Islam, M.T., Chittoori, B.C.S., Burbank, M., 2020. Evaluating the applicability of biostimulated calcium carbonate precipitation to stabilize clayey soils. J. Mater. Civ. Eng. 32 (3), 04019369. https://doi.org/10.1061/(ASCE)MT.1943-5533.0003036.

Jiang, N.-J., Soga, K., 2017. The applicability of microbially induced calcite precipitation (MICP) for internal erosion control in gravel–sand mixtures. Géotechnique 67 (1), 42–55. https://doi.org/10.1680/jgeot.15.P.182.

Jiang, N.-J., Liu, R., Du, Y.-J., Bi, Y.-Z., 2019. Microbial induced carbonate precipitation for immobilizing Pb contaminants: toxic effects on bacterial activity and immobilization efficiency. Sci. Total Environ. 672, 722–731. https://doi.org/10.1016/j.scitotenv.2019.03.294.

Karol, R.H., 2003. Chemical Grouting and Soil Stabilization, Revised and Expanded (0 ed.). CRC Press. https://doi.org/10.1201/9780203911815.

Knorst, M.T., Neubert, R., Wohlrab, W., 1997. Analytical methods for measuring urea in pharmaceutical formulations. J. Pharm. Biomed. Anal. 15 (11), 1627–1632. https://doi.org/10.1016/S0731-7085(96)01978-4.

Kumari, D., Qian, X.-Y., Pan, X., Achal, V., Li, Q., Gadd, G.M., 2016. Microbially-induced carbonate precipitation for immobilization of toxic metals. In: Advances in Applied Microbiology, vol. 94. Elsevier, pp. 79–108. https://doi.org/10.1016/bs.aambs.2015.12.002.

Lee, M., Kolbus, C.M., Yepez, A.D., Gomez, M.G., 2019. Investigating ammonium by-product removal following stimulated ureolytic microbially-induced calcite precipitation. Geo-Congress 2019, 260–272. https://doi.org/10.1061/9780784482117.026.

Lee, M., Gomez, M.G., El Kortbawi, M., Ziotopoulou, K., 2022. Effect of light biocementation on the liquefaction triggering and post-triggering behavior of loose sands. J. Geotech. Geoenviron. 148 (1), 04021170. https://doi.org/10.1061/(ASCE)GT.1943-5606.0002707.

Martinez, B.C., DeJong, J.T., Ginn, T.R., 2014. Bio-geochemical reactive transport modeling of microbial induced calcite precipitation to predict the treatment of sand in one-dimensional flow. Computers and Geotechnics 58, 1–13.

Minto, J.M., MacLachlan, E., El Mountassir, G., Lunn, R.J., 2016. Rock fracture grouting with microbially induced carbonate precipitation: rock fracture grouting with MICP. Water Resour. Res. 52 (11), 8827–8844. https://doi.org/10.1002/2016WR018884.

Minto, J.M., Tan, Q., Lunn, R.J., El Mountassir, G., Guo, H., Cheng, X., 2018. 'Microbial mortar'-restoration of degraded marble structures with microbially induced carbonate precipitation. Constr. Build. Mater. 180, 44–54. https://doi.org/10.1016/j.conbuildmat.2018.05.200.

Minto, J.M., Lunn, R.J., El Mountassir, G., 2019. Development of a reactive transport model for field-scale simulation of microbially induced carbonate precipitation. Water Resour. Res. 55 (8), 7229–7245. https://doi.org/10.1029/2019WR025153.
Montoya, B.M., DeJong, J.T., 2015. Stress-strain behavior of sands cemented by microbially induced calcite precipitation. J. Geotech. Geoenviron. 141 (6), 04015019. https://doi.org/10.1061/(ASCE)GT.1943-5606.0001302.
Montoya, B.M., Gerhard, R., DeJong, J.T., Wilson, D.W., Weil, M.H., Martinez, B.C., Pederson, L., 2012. Fabrication, operation, and health monitoring of bender elements for aggressive environments. Geotech. Test. J. 35 (5), 103300 https://doi.org/10.1520/GTJ103300.
Montoya, B.M., DeJong, J.T., Boulanger, R.W., 2013. Dynamic response of liquefiable sand improved by microbial-induced calcite precipitation. Géotechnique 63 (4), 302–312. https://doi.org/10.1680/bcmpge.60531.012.
Montoya, B.M., Do, J., Gabr, M.M., 2018. Erodibility of microbial induced carbonate precipitation-stabilized sand under submerged impinging jet. IFCEE 2018, 19–28. https://doi.org/10.1061/9780784481592.003.
Montoya, B.M., Do, J., Gabr, M.A., 2021. Distribution and properties of microbially induced carbonate precipitation in underwater sand bed. J. Geotech. Geoenviron. 147 (10), 04021098. https://doi.org/10.1061/(ASCE)GT.1943-5606.0002607.
Mujah, D., Shahin, M.A., Cheng, L., 2017. State-of-the-art review of biocementation by microbially induced calcite precipitation (MICP) for soil stabilization. Geomicrobiol J. 34 (6), 524–537. https://doi.org/10.1080/01490451.2016.1225866.
Nafisi, A., Montoya, B.M., Evans, T.M., 2020. Shear strength envelopes of biocemented sands with varying particle size and cementation level. J. Geotech. Geoenviron. 146 (3), 04020002. https://doi.org/10.1061/(ASCE)GT.1943-5606.0002201.
Nassar, M.K., Gurung, D., Bastani, M., Ginn, T.R., Shafei, B., Gomez, M.G., Graddy, C.M. R., Nelson, D.C., DeJong, J.T., 2018. Large-scale experiments in microbially induced calcite precipitation (MICP): reactive transport model development and prediction. Water Resour. Res. 54 (1), 480–500. https://doi.org/10.1002/2017WR021488.
Parkhurst, D.L., Appelo, C.A.J., 2013. Description of input and examples for PHREEQC version 3–A computer program for speciation, batch-reaction, one-dimensional transport, and inverse geochemical calculations. In: U.S. Geological Survey Techniques and Methods, book 6, chap. A43, p. 497.
Phillips, A.J., Cunningham, A.B., Gerlach, R., Hiebert, R., Hwang, C., Lomans, B.P., Westrich, J., Mantilla, C., Kirksey, J., Esposito, R., Spangler, L., 2016. Fracture sealing with microbially-induced calcium carbonate precipitation: a field study. Environ. Sci. Technol. 50 (7), 4111–4117. https://doi.org/10.1021/acs.est.5b05559.
Phillips, A.J., Troyer, E., Hiebert, R., Kirkland, C., Gerlach, R., Cunningham, A.B., Spangler, L., Kirksey, J., Rowe, W., Esposito, R., 2018. Enhancing wellbore cement integrity with microbially induced calcite precipitation (MICP): a field scale demonstration. J. Pet. Sci. Eng. 171, 1141–1148. https://doi.org/10.1016/j.petrol.2018.08.012.
Ramakrishnan, V., Panchalan, R.K., Bang, S.S., City, R., 2005. Improvement of concrete durability by bacterial mineral precipitation. In: Proc. ICF, 11, pp. 357–367.
Riveros, G.A., Sadrekarimi, A., 2020. Liquefaction resistance of Fraser River sand improved by a microbially-induced cementation. Soil Dyn. Earthq. Eng. 131, 106034 https://doi.org/10.1016/j.soildyn.2020.106034.
Safdar, M.U., Mavroulidou, M., Gunn, M.J., Purchase, D., Gray, C., Payne, I., Garelick, J., 2021. Towards the development of sustainable ground improvement techniques—biocementation study of an organic soil. Circ. Econ. Sustain. 1–26.
San Pablo, A.C.M., Lee, M., Graddy, C.M.R., Kolbus, C.M., Khan, M., Zamani, A., Martin, N., Acuff, C., DeJong, J.T., Gomez, M.G., Nelson, D.C., 2020. Meter-scale biocementation experiments to advance process control and reduce impacts: examining spatial control, ammonium by-product removal, and chemical reductions. J. Geotech. Geoenviron. 146 (11), 04020125. https://doi.org/10.1061/(ASCE)GT.1943-5606.0002377.
San Pablo, A.C.M., Graddy, C.M.R., DeJong, J.T., Gomez, M.G., Nelson, D.C., 2022. Solution Optimization of Stimulated Microbially Induced Calcite Precipitation (MICP) for up-Scaling by Reduction of Urea Inputs (To Be Submitted).
Saneiyan, S., Ntarlagiannis, D., Ohan, J., Lee, J., Colwell, F., Burns, S., 2019. Induced polarization as a monitoring tool for in-situ microbial induced carbonate precipitation (MICP) processes. Ecol. Eng. 127, 36–47. https://doi.org/10.1016/j.ecoleng.2018.11.010.
Seagren, E.A., Aydilek, A.H., 2010. Bioremediated geomechanical processes. In: Mitchell, R., Gu, J.-D. (Eds.), Environmental Microbiology. John Wiley & Sons, Inc., pp. 319–348. https://doi.org/10.1002/9780470495117.ch14
Sharma, M., Satyam, N., Reddy, K.R., 2021. State of the art review of emerging and biogeotechnical methods for liquefaction mitigation in sands. J. Hazard. Toxic Radioact. Waste 25 (1), 03120002. https://doi.org/10.1061/(ASCE)HZ.2153-5515.0000557.
Stocks-Fischer, S., Galinat, J.K., Bang, S.S., 1999. Microbiological precipitation of CaCO3. Soil Biol. Biochem. 31 (11), 1563–1571. https://doi.org/10.1016/S0038-0717(99)00082-6.
Terzis, D., Laloui, L., Dornberger, S., Harran, R., 2020. A full-scale application of slope stabilization via calcite bio-mineralization followed by long-term GIS surveillance. Geo-Congress 2020, 65–73. https://doi.org/10.1061/9780784482834.008.
Tobler, D.J., Cuthbert, M.O., Greswell, R.B., Riley, M.S., Renshaw, J.C., Handley-Sidhu, S., Phoenix, V.R., 2011. Comparison of rates of ureolysis between *Sporosarcina pasteurii* and an indigenous groundwater community under conditions required to precipitate large volumes of calcite. Geochim. Cosmochim. Acta 75 (11), 3290–3301. https://doi.org/10.1016/j.gca.2011.03.023.
Tobler, D.J., Cuthbert, M.O., Phoenix, V.R., 2014. Transport of *Sporosarcina pasteurii* in sandstone and its significance for subsurface engineering technologies. Appl. Geochem. 42, 38–44. https://doi.org/10.1016/j.apgeochem.2014.01.004.
Tziviloglou, E., Wiktor, V., Jonkers, H.M., Schlangen, E., 2016. Bacteria-based self-healing concrete to increase liquid tightness of cracks. Constr. Build. Mater. 122, 118–125. https://doi.org/10.1016/j.conbuildmat.2016.06.080.
van Paassen, L.A., 2009. Biogrout: Ground Improvement by Microbially Induced Carbonate Precipitation. Ph.D. thesis.. Delft University of Technology, Delft.
Wang, Y.-J., Han, X.-L., Jiang, N.-J., Wang, J., Feng, J., 2020. The effect of enrichment media on the stimulation of native ureolytic bacteria in calcareous sand. Int. J. Environ. Sci. Technol. 17 (3), 1795–1808. https://doi.org/10.1007/s13762-019-02541-x.
Xiao, P., Liu, H., Xiao, Y., Stuedlein, A.W., Evans, T.M., 2018. Liquefaction resistance of bio-cemented calcareous sand. Soil Dyn. Earthq. Eng. 107, 9–19. https://doi.org/10.1016/j.soildyn.2018.01.008.
Xiao, Y., Wang, Y., Wang, S., Evans, T.M., Stuedlein, A.W., Chu, J., Liu, H., 2021. Homogeneity and mechanical behaviors of sands improved by a temperature-controlled one-phase MICP method. Acta Geotech. 16 (5), 1417–1427. https://doi.org/10.1007/s11440-020-01122-4.
Zamani, A., Montoya, B.M., 2019. Undrained cyclic response of silty sands improved by microbial induced calcium carbonate precipitation. Soil Dyn. Earthq. Eng. 120, 436–448. https://doi.org/10.1016/j.soildyn.2019.01.010.
Zambare, N.M., Lauchnor, E.G., Gerlach, R., 2019. Controlling the distribution of microbially precipitated calcium carbonate in radial flow environments. Environ. Sci. Technol. 53 (10), 5916–5925. https://doi.org/10.1021/acs.est.8b06876.